Energy landscapes in photochemical dissociation of small peroxides

by

Meisam Farzalipour Tabriz

A Thesis Submitted to the
Graduate School of Sciences and Engineering
in Partial Fulfillment of the Requirements for
the Degree of

Master of Science
in
Materials Science and Engineering

Koç University
June 2015

Koç University
Graduate School of Sciences and Engineering

This is to certify that I have examined this copy of a master's thesis by

Meisam Farzalipour Tabriz

and have found that it is complete and satisfactory in all respects,
and that any and all revisions required by the final
examining committee have been made.

Committee Members:

_____

Ersin Yurtsever, Ph. D. (Advisor)

_____

Özgür Birer, Ph. D.

_____

Nurcan Tüzün, Ph. D.

Date: _____

ABSTRACT

Organic peroxides are known to have important roles in many chemical and biochemical processes e.g. as intermediates in the oxidation of various hydrocarbons with oxygen, as initiators of free-radical polymerization and cross-linking agents, in lipid oxidation, and in DNA damage and mutation. Thus, study of the organic peroxides and their radicals are of fundamental interest and importance. Although several reaction pathways after dissociation of organic peroxides have been successfully identified using time-resolved optical absorption spectra, interpretation of these data can be complicated due to spectral overlap of parent molecules, intermediates, and products. Therefore, a combined experimental-theoretical investigation is necessary in case of complex or less studied systems.

In this study, we tried to identify the thermal dissociation pathways in photodissociation of diethyl peroxide, di-tert-butyl peroxide and dicumyl peroxide by locating all local minima and the connecting transition states in their photochemical dissociation.

We used DFT approach with M06-2X functional which was found to be suitable for calculations of equilibrium geometries, relative energies and electronic excitation energy values. We compared calculated DFT energies with CCSD(T) level energies which was shown to have no additional information.

As observed experimentally, methyl radical abstraction is the main dissociation mechanism for studied peroxides after O-O bond breaking. This reaction was found to have the least activation energy in all studied peroxides.

By locating all local minima and transition states for the secondary reactions, we are able to construct the energy landscapes of the peroxide dissociation and their general characteristics.

For our results to be comparable to experimental time-resolved UV-Vis absorption spectra, we used TDDFT/PCM method for calculating electronic excitation energies in

the presence of acetonitrile and ethanol solvents. Shifts in electronic excitation energies of studied radicals in these solvents were found to be similar and negligible.

ÖZET

Organik peroksitler, birçok kimyasal ve biyokimyasal süreçte karşımıza çıkmaktadırlar. Örneğin; hidrokarbonların oksidasyonundaki ara ürünler, serbest radikal polimerizasyon başlatıcıları, çapraz bağlama maddeleri gibi malzemelerde, lipid oksidasyonunda, DNA hasarı ve mutasyonunda peroksitler önemli rol oynamaktadırlar. Bu nedenle, organik peroksitler ve bunlardan oluşan radikallerinin anlaşılması önemli bir problem oluşturmaktadır. Her ne kadar bazı organik peroksitlerin bozunmalarından oluşan tepkimelerin mekanizmaları, zamana bağlı optik spektroskopik yöntemlerle anlaşılmış ise de, bu verilerin yorumlanması ana moleküllerin, ara ürünlerin ve son ürünlerin spektrumlarının örtüşmesi nedeniyle çok zor olmaktadır. Bu durumda, hem daha karmaşık hem de nispeten az çalışılmış sistemlerin teorik ve deneysel incelemelerinin yapılması ve birleştirilmesi gerekmektedir.

Bu çalışmada, dietil peroksit, di-tert-butil peroksit ve dikümil peroksit için fotokimyasal bozulma esnasında oluşabilecek tüm yerel minima ve geçiş hallerini belirleyerek parçalanma ve ötesindeki tepkime mekanizmalarını saptamaya çalıştık.

M06-2X fonksiyoneli kullanılarak yapılan DFT hesaplarının denge konumlarının bulduğu, göreceli enerjileri ve elektron uyarılma enerji değerlerini oldukça doğru hesapladığı hem literatürde verilmiştir hem de hesaplarımızda gözledik. Hesapladığımız DFT enerjilerini CCSD(T) enerjileri ile karşılaştırdık ve CCSD(T) enerjilerinin herhangi bir ek bilgi sağlamadığını gösterdik.

Deneysel olarak da gözlemlendiği gibi, metil radikalinin çıkışı incelediğimiz peroksitlerde O-O bağlarının kırılmasından sonraki temel tepkimedir. Bu tepkime incelenen tüm peroksitlerde en düşük aktivasyon enerjisine sahiptir.

İkincil tepkimelerde oluşabilecek bütün minimum enerji yapıları ve geçiş hallerini bularak, peroksit parçalanmalarındaki enerji haritalarını ve bunların genel davranışlarını elde ettik.

Sonuçlarımızın zamana bağlı alınan optik spektrumları ile karşılaştırabilir olması için, asetonitril ve etanol çözeltileri içindeki elektron uyarılma enerjilerinin hesaplanmasında

TDDFT/PCM metodu kullanıldı. İncelenen radikallerin bu çözeltiler içerisindeki elektron uyarılma enerjilerindeki kaymalarının benzer ve ihmal edilebilir olduğu bulundu.

ACKNOWLEDGEMENTS

I would like to most sincerely thank my advisor, Prof. Dr. Ersin Yurtsever, for his constant guidance, unlimited patience in teaching me quantum chemistry and his unbelievable energy and support during the works on my thesis.

I would like to thank Asst. Prof. Dr. Özgür Birer for motivating and directing me to Prof. Yurtsever at the beginning of my master's studies and also for his insights into the reaction mechanisms, valuable comments and suggestions, and providing experimental data.

I would also like to thank Prof. Dr. Volker Staemmler (Ruhr-University Bochum) and Prof. Dr. Willem M. Klopper (Karlsruhe Institute of Technology) from whom I had the opportunity of learning many useful concepts and methods in theoretical/computational chemistry.

My special thanks go to my beloved friends Artür Manukyan and Hassan Babaei for having fruitful discussions on computational science and quantum physics and Vahdet Ünal for helping me in preparing the Turkish abstract.

I want to express my gratitude to Hüseyin Özbey for his helps in running my calculations on Koç university cluster.

I acknowledge the financial support of the Scientific and Technological Research Council of Turkey (TÜBİTAK-113Z211) during my master's study.

TABLE OF CONTENTS

LIST OF TABLES

LIST OF FIGURES

Chapter 1

INTRODUCTION

1.1 Organic peroxides

Organic peroxides are chemical compounds with one or more O-O bonds. They can be considered as derivatives of hydrogen peroxide in which the hydrogens are substituted by organic groups (ROOR') [1].

Studies of the organic peroxides and their radicals are of fundamental interest and importance due to their role as intermediates in the oxidation of hydrocarbons with molecular oxygen [2], as initiators of free-radical polymerization [3], and as cross-linking agents [4]. They are also involved in many biochemical processes such as lipid oxidation [5], and DNA damage and mutation [6; 7]. Therefore, various aspects of their structures [8], thermochemical properties [9], and dissociation [10] have been studied over the years by many researchers.

The characteristic feature of peroxide compounds is their weak [11] covalent O-O bond which makes them thermochemically and photolytically unstable. Extensive literature exists on thermal peroxides decomposition [12-16]. But, it was only recently that development in ultra-fast laser techniques made it possible to study the unimolecular photo-dissociation of the molecules and consecutive reactions with sufficient resolution in femto-/pico-second time scale [17]. It is already established that this approach can be successfully employed for investigation of reactions in organic peroxides [18]. But currently most of the literature in this field are limited to diaroyl peroxides, peroxyesters, and peroxycarbonates [19-22].

Although several reaction pathways after dissociation of organic peroxides have been successfully identified using time-resolved optical absorption spectra, interpretation of these data can be complicated due to spectral overlap of parent molecules, intermediates, and products. Consequently, a combined experimental-theoretical investigation is necessary in case of complex or less studied systems [23; 24].

Our goal in this study is to identify the thermal dissociation pathways by locating all local minima and the connecting transition states which may be produced during the photochemical dissociation of few important organic peroxides. The energy landscapes of these processes are studied by accurate quantum chemical calculations.

1.2 Quantum calculations

1.2.1 Time-independent non-relativistic Schrödinger equation

The main goal the of most quantum chemical approaches is to find the approximate solution of time-independent, non-relativistic Schrödinger equation [25]:

$$\hat{H}\psi = E\psi \tag{1.1}$$

where, $\hat{H}$ is the Hamilton operator for a molecular system consisting of M nuclei and N electrons in the absence of magnetic or electric fields, Ψ is the total wave function and E is energy eigenvalue.

1.2.2 Born–Oppenheimer approximation

Born–Oppenheimer approximation [26] states that, the motion of electrons in a molecule is much faster than that of the nuclei, therefore we can assume the positions of nuclei to be fixed in our calculations. This means that we can separate the nuclear and electronic terms in the Schrödinger equation and solve the equation for nuclei with fixed positions. Thus, only the electronic part of complete Hamiltonian (eq. 1.1) is relevant:

$$\hat{H}_{elec} = -\frac{1}{2}\sum_{i=1}^{N}\nabla_i^2 - \sum_{i=1}^{N}\sum_{A=1}^{M}\frac{Z_A}{r_{iA}} + \sum_{i=1}^{N}\sum_{j>i}^{N}\frac{1}{r_{ij}} \quad (1.2)$$

where, ∇_i^2 is the Laplacian operator for the i-th electron, Z_A is the nuclear charge of atom A, r_{iA} is distance between the nucleus A and electron i and r_{ij} is the distance between electrons i and j. The solution of the Schrödinger equation with electronic Hamiltonian ($\hat{H}_{elec}$) is the electronic wave function (Ψ_{elec}) and the electronic energy (E_{elec}).

$$\hat{H}_{elec}\psi_{elec} = E_{elec}\psi_{elec} \quad (1.3)$$

1.2.3 Hartree-Fock approximation

We need further approximations to solve the obtained electronic Schrödinger equation. The simplest one is to assume electrons move independent of each other. Hartree-Fock (HF) approximation [27; 28] is method of approximating the N-electron wave function solution of (eq. 1.3) by an antisymmetrized product of N orthonormal one-electron wave functions (spin-orbital). This product is called Slater determinant [29]:

$$\psi = \frac{1}{\sqrt{N!}}\begin{vmatrix} \chi_1(1) & \chi_2(1) & \cdots & \chi_n(1) \\ \chi_1(2) & \chi_2(2) & \cdots & \chi_n(2) \\ \vdots & \vdots & \ddots & \vdots \\ \chi_1(N) & \chi_2(N) & \cdots & \chi_n(N) \end{vmatrix} \quad (1.4)$$

where, χ_i is a spin-orbital which is product of spatial orbital and a spin function. Slater determinants automatically ensures that we are obeying the Pauli exclusion principle [30], by collapsing wave function when any two electrons in a system have the same quantum numbers.

Initial guess for calculations can be obtained by various methods such as using Harris functional [31] or extended Hückel method [32]. Then, self-consistent-field equations (SCF) [33; 34] can be used to get a set of molecular orbitals with lower

expectation value of the Hamiltonian operator ($E = \langle \psi | \hat{H} | \psi \rangle$) which according to variational principle [35] is a better representative of system than the initial guess. SCF procedure repeats until the generating orbitals get self-consistent with the Fock matrix they are generated from.

Although the results obtained from HF method are very useful in many situations, it is not always quantitatively or sometimes even qualitatively correct. Lots of different methods have been developed to recover the missing electron correlation in HF approximation for improving the accuracy of its results. Møller–Plesset perturbation theory (MP) [36], configuration interaction (CI) [37], and coupled-cluster (CC) approaches [38; 39] are a few of these attempts.

1.2.4 Density functional theory

Density functional theory (DFT) provides a conceptually alternative approach to include electron correlation. In DFT, the many-body effect of electron correlation is modeled by a function of the electron density instead of the many-electron wave function.

Hohenberg and Kohn [40] were first to show that electronic ground state energy from Schrödinger equation is a unique functional of the electron density. They also proved that this functional is variational. The ground state electronic energy of a system composed of n electrons and N nuclei in Kohn-Sham formalism [41] can be written as:

$$E[\rho] = -\frac{1}{2}\sum_{i=1}^{n}\int \psi_i^*(r_1)\nabla_i^2\psi_i(r_1)dr_1 - \sum_{X=1}^{N}\int \frac{Z_X}{r_{Xi}}\rho(r_1)dr_1 + \frac{1}{2}\iint \frac{\rho(r_1)\rho(r_2)}{r_{12}}dr_1dr_2 + E^{XC}[\rho] \quad (1.5)$$

where, Ψ_i are the Kohn-Sham orbitals, the first term is kinetic energy of the electrons by neglecting their interactions, the second term is due to nucleus-electron interactions, the third term accounts for the Columbic repulsions between two charge distributions positioned at r_1 and r_2, and the last term, known as the exchange-

correlation (XC) is correction to the kinetic energy due to electrons interactions, and also all non-classic corrections to the electron-electron repulsion energy.

DFT in the Kohn–Sham formulation is formally an exact many-body quantum mechanical theory for the ground-electronic-state properties of a system. However, it depends on an unknown ("very complicated and essentially uncomputable" [42]) universal XC functional (density functional) that can only be approximated. One may write XC as a separable function $E^{XC}[\rho] = E^{X}[\rho] + E^{C}[\rho]$ in which the exchange energy (E^X) part of functional corrects the spurious self-interaction of one electron with itself while the correlation energy (E^C) part accounts for the effects of Coulomb correlation upon the many electron wave function [43].

DFT approach can be viewed as method to converts an eigenvalue problem from 3N into just 3 spatial coordinates. The most important advantage of using DFT instead of HF calculations is its ability to get reliable results with significant improvement over those obtained from the HF in a comparable time [44].

Conventional formulations of SCF theory, such as the Roothaan-Hall [33; 34] and Kohn-Sham [41] methods involve N^3 Eigen solution of an effective single-particle Hamiltonian or Fockian in an orthogonal representation, where N is the number of basis functions. The computational cost of a HF calculation is dominated by the N^4 cost of constructing the Fock matrix, but in large systems where the diagonalization step is the limiting process, it ultimately reduces to $N^{\sim 3}$ [45]. Calculation of Fock matrix is also the limiting factor in the hybrid HF/DFT treatment of large systems [46]. Although numerous algorithms have been developed for decreasing the necessary computational effort in DFT and HF calculations, but still in most of the modern quantum chemistry packages both of these methods have more or less similar computational complexity [47].

1.2.5 DFT functionals

The local density approximation (LDA) is the simplest approach to represent the XC functional. In this approach, the XC energy at any point in space is assumed as only a

function of the electron density at the same point in space. A homogeneous electron gas of the same density is used for these calculations [41].

Generalized gradient approximation (GGA) methods account for spatial inhomogeneity of electron density by making the XC energies dependent on the density and its gradient in space [48]. Non-separable gradient approximation (NGA) methods have the same assumptions as GGA but their XC term is not separable [49].

Meta-GGA (mGGA) functionals depend on higher orders of electron density gradients, or the kinetic energy density, which incorporates derivatives of the occupied Kohn-Sham orbitals into the XC [50].

Hybrid density functional (hGGA) methods combine the XC of a GGA method with a predefined percentage of HF exchange [51]. This amount is considered to be constant in global hybrid functionals but range-separated hybrid functionals consider it to be different for short-range and long-range interactions based on the inter-electronic distance [52].

Hybrid-meta GGA methods (hmGGA) are hybrid density functionals which use mGGAs instead of standard GGAs. Thus, these functionals depend on the HF exchange, the electron density and its gradient, and the kinetic energy density [53].

1.2.6 Basis set

Electronic structure calculations on molecules make the assumption that molecular wave functions can be represented as the linear combination of atomic orbitals (LCAO) [54].

A basis set contains a finite number of basis functions which is used for combination to give the molecular wave functions. The minimal basis set is the set that incorporates only the orbitals actually populated by electrons.

Nuclear-centered Slater [55] or Gaussian-type functions [56] are two of the most widely used function types for molecular systems. The resulted orbitals using these functions are named as Slater type orbital (STO), and Gaussian type orbital (GTO), respectively. Although STO exhibits the correct discontinuous derivative (Kato's cusp

condition [57]) at $r \rightarrow 0$, unlike GTO which has a slope of zero at this point, but Gaussian functions are preferred due to existence of analytical solutions for calculations of three- and four-center two-electron integrals.

Currently, the most widely used Gaussian basis sets are Pople basis sets [58; 59], correlation-consistent basis sets [60; 61], and Karlsruhe basis sets [62].

1.2.7 Geometry optimization

In quantum chemical calculations usually the first step requires optimization of the molecular geometry to find characteristic stationary point structures (e.g. equilibrium geometry, transition state structure, etc.) on potential energy surface (PES).

1.2.7.1 Equilibrium geometry

Equilibrium geometry of a molecule is considered as minima on the PES. There are three general categories of optimization methods for finding these minima. These methods depend on local slopes (gradients) of PES and/or its curvatures (Hessians):

1. Steepest descent: A series of energy evaluations are done in negative gradient direction. Once the energy starts to increase, approximate minimum can be found by interpolation between the calculated points on PES [63].
2. Conjugated gradient: In each step, a new search direction is chosen such that it lowers the energy while staying at or near the minimum in the earlier followed search direction [64].
3. Newton-Raphson: PES is approximated by a local quadratic function and its minimum is found in the steepest descent direction. But as the PES is usually non-quadratic, minimization of energy on approximated PES must be done iteratively in order to converge to a minimum [65].

Various optimization algorithms based on natural [66], redundant [67], or delocalized [68] internal coordinates have been already developed. Using these coordinate for optimization of molecular geometries is generally much more efficient than using Cartesian coordinates system. The efficiency of different methods can be

compared based on the number of optimization cycles needed to find a stationary point [69; 70].

Once a minimum energy configuration is found, the eigenvalues of the Hessian at this geometry must be computed. At a true local minimum, all eigenvalues must be positive.

1.2.7.2 Transition state

To find the geometry of transition states of a chemical reaction, one must find a geometry corresponding to a point on PES which satisfies the following criteria [71]:

1. It must be a stationary point.
2. The force constant matrix at that point must have one and only one negative eigenvalue.
3. It must be the highest energy point on a continuous line connecting reactants and products to each other.
4. It must be the lowest energy point which satisfies all the three conditions above.

There are various optimization methods for finding TS. The most successful ones include reaction coordinate approach, synchronous transit, and quasi-Newton methods [72].

Reaction coordinate approach, tries to find the minimum energy path (MEP) between the reactants and products. All the maxima along the MEP are saddle points on the PES, and the energy of the highest saddle point defines the minimum required energy for the reaction or by definition the activation energy [73].

In the synchronous transit approach, a series of energy calculations are performed on a set of structures with parameters which are linearly interpolated between a given reactant and product (linear synchronous transit). The structure with the highest energy along this path provides a first estimate of the transition state structure and its energy difference can be considered as activation energy. Then, search in orthogonal direction to the linear synchronous transit path is performed to find an intermediate for defining a quadratic synchronous transit pathway [74].

Quasi-Newton methods for finding transition states work exactly like the method for finding minima on PES except that they force the Hessian to contain a single negative eigenvalue [75].

The reaction path can be defined as a line/path on PES which connects the reactants and products via maximum energy point. If we identify the transition state on PES, this path can be easily found by searching for the steepest descent path or MEP from this point toward the reactants and products [76]. If we use mass-weighted Cartesian coordinates, the obtained path is called the intrinsic reaction coordinate (IRC) [77]. Although, IRC is not the real dynamic behavior of the system in reaction (due to neglecting the atomic vibrations), it can be used to verify that this TS does indeed connect the reactants and products of interest [78].

1.2.8 Zero-point vibration energy

Harmonic force constants and consequently vibrational frequencies can be analytically calculated from approximated wave function in ab-initio methods [79; 80] and by using Hellmann-Feynman theorem [81; 82] from electron density in DFT approach [83].

For comparison with experiment, every method for determining thermodynamic quantities based on quantum mechanical procedures ultimately requires the addition of a zero-point vibrational energy (ZPVE) correction to convert the electronic energies (E_{elec}) into 0 K heats of formation ΔH_f^0. ZPVE is calculated for a harmonic oscillator model as the half of the sum of fundamental frequencies [84]:

$$ZPVE = \sum_i \frac{1}{2} hc\nu_i \qquad (1.6)$$

In molecules with large ZPE value, it is essential to go beyond the harmonic approximation to obtain a reliable ZPVE. The anharmonicity of the fundamental frequencies can be accounted for by scaling the obtained harmonic frequencies. This procedure is known to work well due to fairly uniform overestimation of vibrational frequencies [85; 86].

1.2.9 Electronic excitation energy

Prediction of the energies of electronic excited states of molecules and transition probabilities are necessary for interpretation of the UV-Vis absorption spectra. Several approaches are used for calculations of excitation energies of molecular systems. Most common ones which can be used in larger systems are configuration interaction singles (CIS), time-dependent Hartree–Fock (TDHF), and time-dependent density functional theory (TDDFT) [87].

1.2.9.1 Configuration interaction singles

Configuration interaction (CI) approximation is based on the expanding ground-state wave function in the excited determinants formed by swapping one or several occupied orbitals by virtual ones in the Stater determinant. If we move only one electron in each determinant, the resulted approximation is called a configuration interaction single-excitation (CIS). CIS calculations give an approximation to the excited states of the molecule, but according to Brillouin's Theorem [88] do not change the ground-state energy. In general, due to missing electron correlation, CIS excitation energies (like TDHF) are fairly overestimated [89].

1.2.9.2 Time-dependent Hartree-Fock theory

The time-dependent self-consistent field theory (also referred as time-dependent Hartree-Fock theory (TDHF) or random-phase approximation (RPA)) is an approach to find an approximate solution of the time-dependent Schrödinger equation and describing the absorption of radiation [90]. The time-dependent Hartree-Fock equations approximate the exact time-dependent Schrödinger equation by assuming that the system under investigation can be represented by a single Slater determinant composed of time-dependent single-particle wave functions at all times. Generally, TDHF results are not improved significantly over CIS. Thus, its increased computational cost is not well justified.

1.2.9.3 Time-dependent density functional theory

TDDFT is an extension of DFT as another approach to solution of nonrelativistic time-dependent Schrödinger equation. It is based on the Runge-Gross theorem [91] which establishes that in a time-dependent quantum problem, all observables are functionals of the time-dependent density. Considering the linear-response of a molecule to a long-wavelength oscillating electric field as a weak perturbation, one finds simple formulas that correct the KS eigenvalue differences into the optical excitations of the system, but it requires another unknown functional (XC kernel) [92].

TDDFT is very popular in the calculation of excited-state properties due to its ability to give accurate quantitative results for large molecule which unlike correlated wave function-based methods, such as Multi-Reference Configuration Interaction (MRCI) [93], Multi-Configurational Self-Consistent Field (MCSCF) [94], Complete Active-Space SCF (CASCF) [95], and Complete Active Space Second Order Perturbation Theory (CASPT2) [96] can be obtained at a moderate computational cost.

Calculated excitation energies for open-shell systems with the CIS and TDHF methods have large errors due to "the multi-determinantal character of the ground and excited state wave functions of open-shell systems in a HF reference" and instabilities involved [97]. In these cases, TDDFT can be considered as a zeroth-order theory for calculations of valence excited states in radicals [98].

The accuracy of TDDFT highly depends on the employed exchange-correlation functional. Various functionals are known to work well for low-lying valence excited states. In comparison, TDDFT results usually are significantly improved at equivalent computational cost when compared with HF based methods such as CIS and TDHF [99]. TDDFT excitation energies generally have high accuracy with an error in the order of 1 eV or less; except for few well-known cases such as charge transfer, Rydberg states, and double excitations.

TDDFT can be used for molecules in which correlated ab initio methods are too time-consuming [100]. Moreover, several efficient algorithms have been developed form parallel implementation of TDDFT codes [101] which makes it a suitable choice

for bigger molecules. In addition, effects of different solvents on electronic excitation energies can be easily calculated in TD-DFT approach with the help of continuum models [102] to make the calculation results comparable to real world experiments.

1.2.10 Solvent effects

Liquid solutions have important role in chemistry as many of reactions and experiments are done in solutions. In most general case, the effects of solvents can be modeled implicitly by including solvent molecules inside the system under the consideration or explicitly by considering the average effects caused by them using continuum models.

The main advantage of using continuum models is tremendous reduction in the system's number of degrees of freedom. For example, if we treat 100 molecules of water solvent explicitly, with this approach 900 additional degrees of freedom have to be considered for the entire system.

Continuum models based on their approach to determining the solvent reaction potential and its interaction energy with the charge distribution, can be categorized into [103]:

1. Multipole expansion (MPE) methods,
2. Image charge (IC) methods,
3. Apparent surface charge (ASC) methods,
4. Finite element methods (FEM), and
5. Finite difference methods (FDM).

Among these methods, ASC and MPE are the most commonly used.

The ASC methods are based on the calculation of an apparent spread charge on the surface of a cavity, which is acting as a boundary layer between the dielectric solvent and solute molecule. Calculations based on the ASC methods have remarkable results with any shape of cavity and when the solvent is uniform, they give a formally exact solution to the electrostatic problem [104]. Polarizable Continuum Model (PCM) [105] is the oldest ASC method which is constantly improving [106-108]. This model can be

solved efficiently [109] and has been successfully integrated into DFT [110] and TDDFT [102] methods. PCM has been already implemented in various QM computational packages [111-113].

1.2.11 Parallel computation

Neglecting the worst case scenario of non-converging SCF, the HF algorithm requires diagonalizing the M×M Fock matrix at $O(M^3)$ computational cost [114]. Complexity of DFT method in general is dependent on description of its XC functional [114; 115]. Complexity of HF calculations is dominant part of the complexity of DFT calculations using approximate functionals with HF exchange part [116].

Unless more efficient algorithms are found to solve these problems, this complexity of calculations limits our investigations to few-atomic molecules and/or small basis set with current performance of the typical computers. A way for somehow circumventing this obstacle is concurrent use of several processors for our calculations using parallel algorithms.

Many parallel algorithms have been developed for HF/DFT calculations which their implementations in well-known QM calculation packages (e.g. NWChem, TURBOMOLE, Gaussian) show near-linear speedup in parallelization [117-119].

For our calculations, we use a non-uniform memory access (NUMA) machines which consist of two sockets, each with a 10-core Intel® Xeon® E5-2680v2 processor. Processors are consisted of 10 Ivy Bridge EP cores which support hyper-threading. The architecture of machines is shown in figure 1.1.

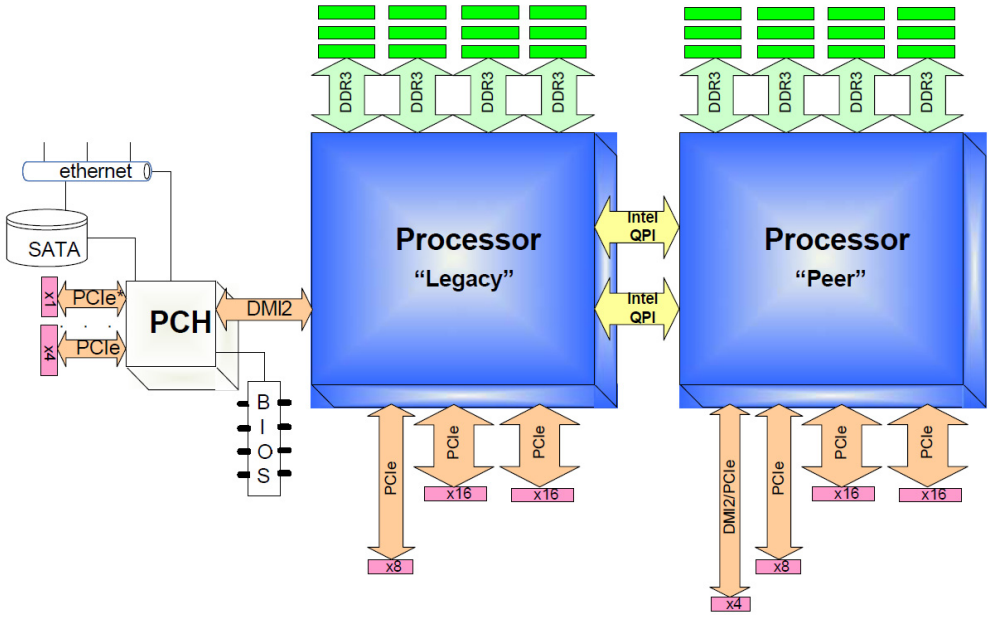

Figure 1.1: Configuration of Intel® Xeon® processor E5-2600 v2 product family on a two socket platform.

1.3 Methodology

1.3.1 Functional

An extensive research in quantum chemistry is devoted to develop new functionals and improve the existing ones. But, the best functional for one application may or may not be the best for a different application [120].

The evaluation of the performance of density functionals by benchmarking for desired properties is a crucial step prior to the investigation of a new system. Our criteria for choosing a functional for our study are its ability to give a reasonably good description of the molecular geometries and bond breaking energies as well as electronic excitation energies. The latter criterion is essential for having comparable results with experimental data from UV-Vis absorption spectra (where applicable).

Probably the most commonly used functional nowadays is hybrid Becke 3 parameter Lee–Yang–Parr [51; 121] (B3LYP) which gives "unexpectedly" good description of the molecular geometries in a reasonable time even with small basis sets [122] which is attributed to systematic error compensation from combining an over-repulsive hybrid GGA part with a (partly over-binding) medium-range correlation part [123].

But despite its popularity, B3LYP is known to have many shortcomings [124; 125], namely in estimation of reaction barrier heights [126; 127] and electronic transition energies [128] both of which are essential for the purpose of our study.

Zhao and Truhlar [129] reported a comparison of the B3LYP with some new developed functionals. Their efforts were focused on solving the problems with transition metals, barrier heights, and weak interactions. They presented Minnesota-06 suit of functionals which "enables computational modeling of diverse chemical phenomena more reliably than was possible previously". The Minnesota functional family currently consists of one mGGA (M06-L [130]), two mNGAs (M11-L [131] and MN12-L [132]), seven global hmGGAs (M05 [133], M05-2X [134], M06-HF [135], M06 [136], M06-2X [136], M08-HX [137] and M08-SO [137]), one range-separated hmGGA (M11 [138]) and one screened-exchange hmNGA (MN12-SX [139]).

Among the current Minnesota functionals, M06-2X functional specifically have been shown to have a good accuracy in calculating both the ground state geometry and excited state energies of main group compounds [129; 140-142] when suitable integration grid is used [143]. It is also a suitable functional for reproducing the experimental excitation band shapes with TD-DFT approach [144].

To illustrate the concept, we compared the accuracy of M06-2X functional in calculations of hydrogen peroxide properties as the simplest peroxide molecule with SVWN [41; 145], BLYP [121; 146], TPSS [50] and B3LYP functionals as representatives from different rungs of Jacob's ladder [147; 148]. Chosen functionals are popular examples of each level of approximation. All calculations in our study are carried out using the Gaussian 09 package (EM64L-G09RevD.01) [149].

The geometry of H_2O_2 molecule is shown in figure 1.2. Parameters for predicted geometry with lowest energy in DFT calculation using each functional are listed in table 1.1.

The experimental equilibrium structure of H_2O_2 molecule has also been an issue of controversy. Dihedral angle θ of hydrogen peroxide have been reported in the literature as, θ~111° [150] and θ~119° [151] from experimental data. This inconsistency was settled by Koput [152] who determined θ=111.83° by solving the torsional Schrödinger equation for a O-H bond distance of 0.965 Å, and fitting his solution to the available experimental data. Later, other studies [153] also confirmed that θ is around the value obtained by Koput. Theoretical studies show that very large basis set (equivalent to aug-cc-pVTZ or larger) is needed to reproduce the experimental geometry parameters for hydrogen peroxide [154].

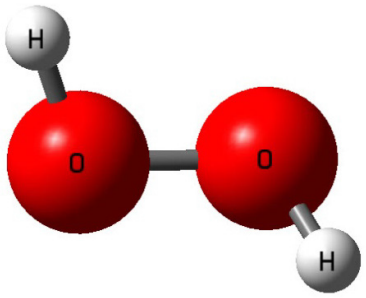

Figure 1.2: Geometry of H_2O_2 molecule ($\alpha = \angle HOO$, θ=HOOH dihedral angle)

Table 1.1: Optimized geometry parameters for H_2O_2 molecule in gas phase with various functionals using aug-cc-pVDZ basis set.

Functional	Type	O-O (Å)	O-H (Å)	α (deg)	θ (deg)
SVWN	LDA	1.429	0.980	101.0	111.1
BLYP	GGA	1.489	0.982	99.7	114.3
TPSS	mGGA	1.475	0.979	99.7	112.9
B3LYP	hGGA	1.451	0.970	100.7	113.3
M06-2X	hmGGA	1.422	0.967	101.5	111.4
Experimental [152; 153]		1.464	0.965	99.4	111.8

We've also calculated the O-O bond dissociation energies with various functionals using a reasonably large (aug-cc-pVDZ) basis set. The energies are corrected for ZPVE and basis set superposition error (BSSE). The full counterpoise (CP) Boys and Bernardi method [155] was used to calculate and correct the energies for the BSSE. The results are listed in table 1.2.

Table 1.2: O-O bond dissociation energies calculated with various functionals using aug-cc-pVDZ basis set.

Functional	Type	O-O bond dissociation energy (kcal/mol)
SVWN	LDA	81.7
BLYP	GGA	50.3
TPSS	mGGA	48.2
B3LYP	hGGA	43.5
M06-2X	hmGGA	46.8
Experimental [156]		48.8

The results for excitation energy of H_2O_2 molecule and ˙OH radical with various functionals using aug-cc-pVDZ basis set are listed in tables 1.3 and 1.4, respectively. Our results show a good agreement of DFT/TDDFT calculations using M06-2X functional with available experimental data.

Table 1.3: Calculated values for first and second excitation energy and oscillator strength of H_2O_2 molecule with various functionals using aug-cc-pVDZ basis set.

Functional	Type	1st Excited State			2nd Excited State		
		ΔE (eV)	λ (nm)	Oscillator strength	ΔE (eV)	λ (nm)	Oscillator strength
SVWN	LDA	5.7014	217.46	0.0085	5.8259	212.82	0.0041
BLYP	GGA	4.9892	248.51	0.0048	5.5667	222.73	0.0032
TPSS	mGGA	5.4428	227.80	0.0057	5.9250	209.25	0.0036
B3LYP	hGGA	5.7066	217.27	0.0050	6.3555	195.08	0.0036
M06-2X	hmGGA	6.0691	204.29	0.0035	6.9075	179.49	0.0037
Experimental [157]		-	-	-	6.8880	180	-

Table 1.4: Calculated values for first and second excitation energy and oscillator strength of ˙OH radical with various functionals using aug-cc-pVDZ basis set.

Functional	Type	1st Excited State		
		ΔE (eV)	λ (nm)	Oscillator strength
SVWN	LDA	3.7982	326.43	0.0011
BLYP	GGA	4.1928	295.70	0.0013
TPSS	mGGA	4.6040	269.30	0.0015
B3LYP	hGGA	4.1920	295.77	0.0014
M06-2X	hmGGA	3.5356	350.67	0.0011
Experimental [158]		4.05	326.84	-

1.3.2 **Basis set**

While using larger basis sets may increase accuracy of the results towards the complete basis set limit [159], but due to polynomial computational complexity order of the most of our calculations, the drastic increase in calculation time may not always make this extra computational effort worthwhile.

For our calculations, we must choose a basis set which provides the best representation of the unknown electron density with as small computational cost as

possible. We investigated the changes in molecular properties, namely, molecular geometry, O-O bond energy, excitation energy, and runtime (as an index of computational cost) for choosing a suitable basis set for our calculations. Changes in geometrical parameters of H_2O_2 molecule by using different basis sets in calculation are listed in table 1.5.

Table 1.5: Optimized geometry parameters for H_2O_2 molecule in gas phase with TDDFT method using M06-2X functional.

Basis set	O-O (Å)	O-H (Å)	α (deg)	θ (deg)
6-31g(d,p)	1.427	0.967	100.7	116.7
6-311g(d,p)	1.424	0.963	101.0	118.3
6-311g(2d,2p)	1.423	0.962	101.1	110.7
cc-pVDZ	1.424	0.970	100.8	115.4
cc-pVTZ	1.424	0.963	101.3	112.7
aug-cc-pVDZ	1.422	0.967	101.5	111.4
aug-cc-pVTZ	1.423	0.964	101.5	112.1
def2-SVP	1.413	0.967	101.4	118.2
def2-TZVP	1.479	0.979	100.4	155.8
Experimental from infrared torsional frequencies [152; 153]	1.464	0.965	99.4	111.8

We calculated O-O bond dissociation energies using M06-2X functional with various basis sets. The energies are corrected for ZPVE and BSSE. The results are listed in table 1.6.

Table 1.6: O-O bond dissociation energies calculated with different basis sets using M06-2X functional.

Basis set	O-O bond dissociation energy (kcal/mol)
6-31g(d,p)	47.1
6-311g(d,p)	44.5
6-311g(2d,2p)	46.6
cc-pVDZ	45.7
cc-pVTZ	47.3
aug-cc-pVDZ	46.8
aug-cc-pVTZ	47.5
def2-SVP	46.7
def2-TZVP	37.6
Experimental [156]	48.8

DFT method with M06-2X functional was used for comparing basis sets due to its accuracy. Using an accurate functional helps us to keep the errors generated due to finite size of basis set from being obscured by the errors inherent to approximations and parameterization of functional.

Calculated excitation energy and oscillator strength of H_2O_2 molecule and $^{\cdot}OH$ radical by using different basis are listed in tables 1.7 and 1.8, respectively.

Table 1.7: Calculated values for first and second excitation energy and oscillator strength of H_2O_2 molecule with TDDFT method using M06-2X functional.

Basis	1st Excited State			2nd Excited State		
	ΔE (eV)	λ (nm)	Oscillator strength	ΔE (eV)	λ (nm)	Oscillator strength
6-31g(d,p)	6.1543	201.46	0.0002	7.6357	162.37	0.0066
6-311g(d,p)	6.0800	203.92	0.0007	7.4751	165.86	0.0030
6-311g(2d,2p)	6.2630	197.96	0.0013	7.4045	167.44	0.0068
cc-pVDZ	6.1442	201.79	0.0006	7.5513	164.19	0.0084
cc-pVTZ	6.2371	198.79	0.0015	7.4605	166.19	0.0090
aug-cc-pVDZ	6.0691	204.29	0.0035	6.9075	179.49	0.0037
aug-cc-pVTZ	6.1320	202.19	0.0034	6.9950	177.25	0.0037

Basis	1st Excited State			2nd Excited State		
	ΔE (eV)	λ (nm)	Oscillator strength	ΔE (eV)	λ (nm)	Oscillator strength
def2-SVP	6.3996	193.74	0.0002	7.6578	161.91	0.0032
def2-TZVP	4.5385	273.18	0.0000	7.0578	175.67	0.0005
Experimental [157]	-	-	-	6.8880	180	-

Table 1.8: Calculated values for first excitation energy and oscillator strength of ˙OH radical with TDDFT method using M06-2X functional.

Basis	1st Excited State		
	ΔE (eV)	λ (nm)	Oscillator strength
6-31g(d,p)	3.6836	336.59	0.0017
6-311g(d,p)	3.6783	337.07	0.0021
6-311g(2d,2p)	3.6718	337.66	0.0014
cc-pVDZ	3.6471	339.95	0.0017
cc-pVTZ	3.6177	342.72	0.0014
aug-cc-pVDZ	3.5356	350.67	0.0011
aug-cc-pVTZ	3.5783	346.49	0.0012
def2-SVP	3.6202	342.48	0.0022
def2-TZVP	3.5082	353.42	0.0037
Experimental [158]	4.05	326.84	-

Performance of TDDFT calculations highly depend on the number of atoms and basis set functions. The amount of time needed for TDDFT calculations as implemented in Gaussian 09 package for first 20 excited states of four simple peroxide molecules on Lufer cluster of Koç University are listed in table 1.9. All calculations are done using 10 threads on physically separate machines.

Table 1.9: Performance of Gaussian 09 package in TDDFT calculations for first 20 excited states on Lufer cluster using 10 nodes.

Molecule	Basis set	No. of basis functions	TDDFT computation time (d:hh:mm:ss)
Dimethyl peroxide	cc-pVDZ	86	00:03:39
Dimethyl peroxide	aug-cc-pVDZ	146	00:11:23
Dimethyl peroxide	cc-pVTZ	204	00:17:17
Dimethyl peroxide	aug-cc-pVTZ	322	01:37:08
Diethyl peroxide	cc-pVDZ	134	00:09:23
Diethyl peroxide	aug-cc-pVDZ	228	00:47:32
Diethyl peroxide	cc-pVTZ	320	01:14:55
Diethyl peroxide	aug-cc-pVTZ	506	07:02:16
Diisopropyl peroxide	cc-pVDZ	182	00:26:54
Diisopropyl peroxide	aug-cc-pVDZ	310	02:06:50
Diisopropyl peroxide	cc-pVTZ	436	03:47:40
Diisopropyl peroxide	aug-cc-pVTZ	690	1:00:47:13
Di-tert-butyl peroxide	cc-pVDZ	230	00:48:53
Di-tert-butyl peroxide	aug-cc-pVDZ	392	04:15:14
Di-tert-butyl peroxide	cc-pVTZ	552	08:02:57
Di-tert-butyl peroxide	aug-cc-pVTZ	874	2:04:57:54

It's already been shown that diffuse augmented basis sets are essential for electronic excitation energy calculations [160]. As it can be seen in table 1.9, by increasing the size of molecule and expanding the basis sets, required time for TDDFT calculation increases. For augmented basis sets which we intend to use, this increment is more drastic. Difference between the results from double-zeta and triple-zeta augmented basis sets (aug-cc-pVDZ and aug-cc-pVTZ) is less than chemical accuracy (commonly defined as ±1 kcal/mol). Thus, we choose aug-cc-pVDZ basis set for our calculations which seems to have sufficient accuracy and highest computational efficiency.

1.3.3 **Geometry optimization**

In our study, we used the Berny algorithm which is a quasi-Newton algorithm with redundant internal coordinates for all of our geometry optimizations which is shown to

work better than Cartesians or non-redundant internals (e.g., Z-matrix coordinates) [161; 162].

For finding transition states geometries, quasi-Newton methods usually have a small radius of convergence because the direction towards the maximum energy on PES is not known in advance and convergence of optimization algorithm to the desired transition state is not guaranteed [163]. We employed synchronous transit-guided quasi-Newton (STGQN) method [164; 165] to find the geometry of transition states. Combined use of synchronous transit and quasi-Newton methods to locate the transition states is proposed as an efficient technique for solving these shortcomings.

We did vibrational frequency analysis on all located transition state geometries to confirm that they have one and only one imaginary frequency and also to get assured that geometry-optimized radicals/molecules have no imaginary frequency and are really corresponding to minima on PES. Also, IRC [166; 167] calculations have been done at the same level to have a verification that the transition states actually connect the intended local minima.

1.3.4 **ZPVE scaling**

We calculated the correction factor of ZPVE for M06-2X method with various basis sets for ZPVE15/10 database [168]. Results of our calculation and experimental values of ZPVEs for molecules in ZPVE15/10 database are listed in table 1.10. ZPVE scaling factor (λ^{ZPE}) can be obtained by least squares method. The reported value for M06-2X/aug-cc-pVTZ method is 0.971 [168] which is consistent with the results of our calculations.

Table 1.10: Calculated ZPVEs for ZVPE15/10 database.

Molecule	ZPVE (kcal/mol)						
	Experimental	M06-2X					
		cc-pVDZ	cc-pVTZ	aug-cc-pVDZ	aug-cc-pVTZ	def2-SVP	def2-TZVP
HF	5.86353	5.90404	5.97340	5.94336	5.94859	5.98787	5.96395
H_2	6.2310	6.42745	6.38760	6.40090	6.38602	6.43122	6.39995
N_2	3.3618	3.63308	3.61000	3.61399	3.60625	3.68931	3.61591
F_2	1.3021	1.59984	1.66441	1.62358	1.66586	1.63750	1.66499
CO	3.0929144	3.25869	3.25236	3.23116	3.24820	3.31955	3.26057
OH	5.2915	5.31491	5.39807	5.37265	5.38893	5.38059	5.38257
Cl_2	0.7983	0.79057	0.82428	0.79641	0.82313	0.75769	0.82748
CO_2	7.3	7.5007	7.50862	7.46746	7.49495	7.61241	7.51148
H_2O	13.26	13.47386	13.54955	13.50555	13.52323	13.54803	13.50037
N_2O	6.770	7.32362	7.29327	7.24470	7.26933	7.42625	7.29079
HCN	10.0	10.49832	10.43009	10.34874	10.42403	10.49883	10.45401
C_2H_2	16.49	17.23816	17.24793	16.87674	17.23681	17.35728	17.22357
H_2CO	16.1	16.9115	16.97116	16.91044	16.95076	17.01054	16.96756
NH_3	21.200	21.59552	21.68515	21.53904	21.63629	21.59266	21.66999
CH_4	27.710	28.0951	28.22651	27.97213	28.21287	28.15171	28.22315
λ^{ZPE}		0.973	0.970	0.979	0.971	0.970	0.971

1.3.5 **UV-Vis absorption spectra**

To calculate excitation energies of our radicals, we did all our TDDFT calculations within the vertical approximation. This means that for estimating the excited state energies we do the calculations using the optimized ground-state geometry. This approximation allows us to do calculations on large systems, as a single-point TDDFT calculation [98].

To simulate absorption spectra from excitation energies, we employed a procedure similar to the one proposed by Stephens and Harada [169]. Generally, the individual peaks in UV/Visible absorption spectra can be described by a Gaussian distribution

function [170]. Thus, we tried to predict the spectrum by fitting calculated excitation energies to Gaussian shaped bands centered at the excitation energies:

$$\varepsilon_i(\tilde{\nu}) = \varepsilon_i^{\max} \exp\left[-\left(\frac{\tilde{\nu}-\tilde{\nu}_i}{\sigma}\right)^2\right] \quad (1.7)$$

where, the i subscript refers to the electronic excitation of interest, $\tilde{\nu}_i$ is the excitation energy (in wavenumbers) corresponding to the electronic excitation of interest. $\varepsilon_i^{\max}$ is the value of ε_i at the maximum of the band: when the energy of the incident radiation $\tilde{\nu}$ is equal to $\tilde{\nu}_i$. σ is the standard deviation in wavenumbers, which is related to the width of the simulated band. This width is related to the decay rate of the state and is affected by various factors such as temperature, solvent, etc.

From the relationship between $\varepsilon_i^{\max}$ and the dipole strength D, (eq. 1.8) and the relationship between the dipole strengths D_i and oscillator strengths, f_i (eq. 1.9):

$$D_i = 4 \times \left[\frac{3 \times 1000 \times h \times c}{32 \times \pi^3 \times N_A}\right] \times \varepsilon_i^{\max} \sqrt{\pi} \frac{\sigma}{\tilde{\nu}_i} \quad (1.8)$$

$$f_i = \frac{8\pi^2 \tilde{\nu}_i m_e c}{3he^2} D_i \quad (1.9)$$

where, N_A is Avogadro's number, c is speed of light, h is Planck's constant, we can rewrite the (eq. 1.7) as:

$$\varepsilon_i(\tilde{\nu}) = 1.3062974 \times 10^8 . \frac{f_i}{\sigma} \exp\left[-\left(\frac{\tilde{\nu}-\tilde{\nu}_i}{\sigma}\right)^2\right] \quad (1.10)$$

where, ε_i is in units of $L.mol^{-1}.cm^{-1}$, and σ is in cm^{-1}. We assume σ to be 0.4 eV ≈ 3226 cm^{-1} which is shown to successfully replicate the experimental spectra [171].

1.3.6 **Parallel computing**

To assess the parallel scalability of Gaussian 09 implementation of TDDFT algorithm on our hardware, we calculated the strong scaling efficiency of TDDFT

calculations on diisopropyl peroxide molecule with M06-2X functional using aug-cc-pVDZ basis set. Results are listed in table 1.11. All calculations are done on separate physical machines to avoid bottle-necks in shared resources. Run-time of each calculation is calculated as the time difference between the start and ending of calculations which consists of time needed for reading input, making scratch files, doing calculations, read/write of data from scratch files, and writing output file. "Total computation time" (T_{tot}) shows the sum of time spend by all thread for calculations. It is possible that some threads stay idle due to imperfect parallelism and/or pipeline saturation, in any stage of computations. The frequency of these events can be measured by "time-usage efficiency" (E_T). "Speedup" (S) is measure of how fast calculations are done in comparison with calculations on a single core (T_1).

$$E_T = T_{tot} / (N \times T_{CN}) \quad (1.11)$$

$$S = T_1 / T_{CN} \quad (1.12)$$

$$E_s = S / N \quad (1.13)$$

where, N is number of simultaneously used threads, T_{CN} is calculation time when job is done with N threads and E_s is strong scaling efficiency.

Table 1.11: Benchmark of Intel Xeon E5-2680v2 processor speedup and scaling efficiency in TDDFT calculations.

Threads number (N)	Run time (hh:mm:ss)	Total computation time (hh:mm:ss)	Time usage efficiency (%)	Speedup	Strong scaling efficiency (%)
1	01:48:31	01:48:24	99.89	1.00	100
2	00:50:43	01:40:58	99.54	2.14	106.98
3	00:35:05	01:44:19	99.11	3.09	103.10
4	00:27:23	01:48:02	98.63	3.96	99.07
5	00:22:09	01:48:50	98.27	4.90	97.98
6	00:19:04	01:52:03	97.95	5.69	94.86
7	00:16:35	01:53:32	97.80	6.54	93.48
8	00:15:34	02:04:03	99.61	6.97	87.14
9	00:13:41	01:59:24	96.95	7.93	88.12
10	00:12:50	02:07:15	99.16	8.46	84.56
11	00:11:47	02:09:01	99.54	9.21	83.72
12	00:10:38	02:02:34	96.06	10.21	85.04
13	00:10:15	02:12:12	99.21	10.59	81.44
14	00:09:35	02:13:28	99.48	11.32	80.88
15	00:09:09	02:16:36	99.53	11.86	79.06
16	00:08:46	02:13:27	95.14	12.38	77.36
17	00:08:24	02:15:26	94.84	12.92	75.99
18	00:08:04	02:17:33	94.73	13.45	74.74
19	00:07:50	02:20:49	94.61	13.85	72.91
20	00:07:45	02:24:07	92.98	14.00	70.01
21	00:07:51	02:35:59	94.62	13.82	65.83
22	00:08:05	02:48:45	94.89	13.42	61.02
23	00:08:03	02:55:29	94.78	13.48	58.61
24	00:08:06	03:03:59	94.64	13.40	55.82
25	00:08:09	03:12:25	94.44	13.31	53.26
30	00:08:20	03:56:23	94.55	13.02	43.41
35	00:08:33	04:42:16	94.32	12.69	36.26
40	00:10:16	06:20:57	92.76	10.57	26.42

As it can be seen in table 1.11, by increasing the number of threads (up to 20), total computation time is increasing. This is mainly due to increasing computational

overhead resulted from increasing the number of communications between each thread and also use of OpenMP barriers for synchronizing the progress of separate threads and generating output files.

In transition from 1 to 2 and 1 to 3 threads, we observe superlinear speedup which can be due to increase of cache and memory bandwidth by automatic placement of threads on different processors which reduces overhead of processors when both of them are being used in comparison to the case where a thread is running on only one of them [172]. Figure 1.3 shows variation of speedup by increasing the threads number on single machine.

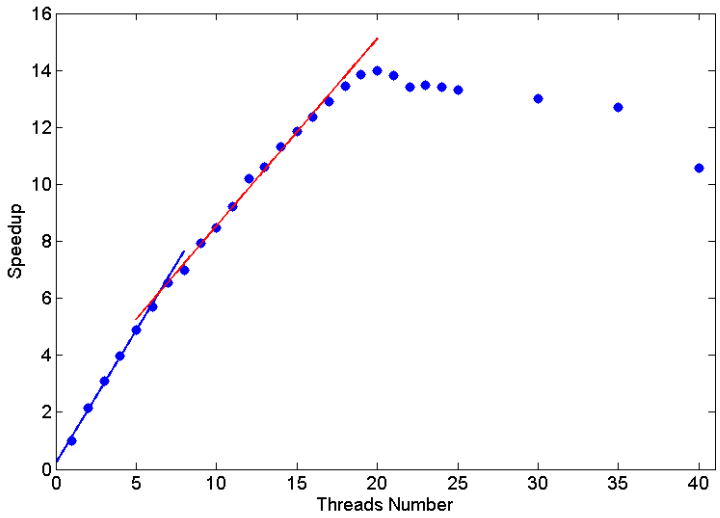

Figure 1.3: Speedup achieved in TDDFT calculations using different number of processing threads.

When there are only few threads running on each processor, Intel Turbo Boost Technology enables processors to perform at a higher frequency than their rated one [173] which is shown in figure 1.3 by blue line. By adding more and more threads to processors and using multiple cores concurrently, due to high power consumption and heat generated by them, the Turbo Boost will be deactivated and processors switch back

to their normal frequency. This performance drop changes the slope of speedup rate (red line).

According to Gustafson-Barsis law [174], by increasing the number of processors, speedup should be monotonically increasing. But in our case, by using more than 20 threads, we see drop in speedup which is due to using Hyper-Threading for doing calculations of 2 threads on a single core. Load latencies, cache misses, branching and dependencies between instructions make Hyper-Threading ineffective [175] and overhead imposed by extra communication and synchronization between the threads leads to lower speedup.

Chapter 2

CALCULATIONS

2.1 Diethyl peroxide

We studied diethyl peroxide dissociation as the simplest model for understanding the possible reactions after dissociation of more complex peroxides of our interest. Thermal decomposition of diethyl peroxide is a unimolecular reaction [176] which makes experimental data comparable to laser-induced half-collision unimolecular dissociation process [177].

Experiments show [178] that the main reactions involved in decomposition of diethyl peroxide are:

$C_2H_5OOC_2H_5 \rightarrow 2C_2H_5O^{\cdot}$ (2.1)

$C_2H_5O^{\cdot} \rightarrow {}^{\cdot}CH_3+CH_2O$ (2.2)

$2\,{}^{\cdot}CH_3 \rightarrow C_2H_6$ (2.3)

Staring from ethyloxidanyl radical ($C_2H_5O^{\cdot}$), we tried to identify the possible products and activation energy of each reaction based on TS energies.

We are mainly interested in reactions including atom abstraction, radical center movement, and further dissociation of peroxide radical. We only consider dissociations with bond homolysis in which each one of involved atoms retains one of the originally-bonded electrons (eq. 2.4).

$AB \rightarrow A^{\cdot}+B^{\cdot}$ (2.4)

$AB \rightarrow A^{+}+B^{-}$ (2.5)

In contrast, in dissociations with bond heterolysis, both of the electrons involved in the original bond remain with only one of the fragment species (eq. 2.5). Heterolysis is favorable dissociation process in some species containing transition metals [179]. Experiments show that typical heterolytic bond dissociation energy for organic chain compounds is about 200 kcal/mol [180] which is well above the needed energy for homolysis dissociation in these compounds.

Figure 2.1 shows schematic energy diagram for the possible reactions with relatively low activation energies (<100 kcal/mol) in this system. Chemical structures of the all involved species are listed in table 2.2. ZPVE and BSSE corrected energy of each radical/TS and also energy differences by taking ethyloxidanyl as reference are listed in table 2.2. Unless otherwise stated, we correct all our calculated energies for ZPVE and BSSE. We treated the TSs as independent entities which do not need any BSSE correction with respect to the other unimolecular species.

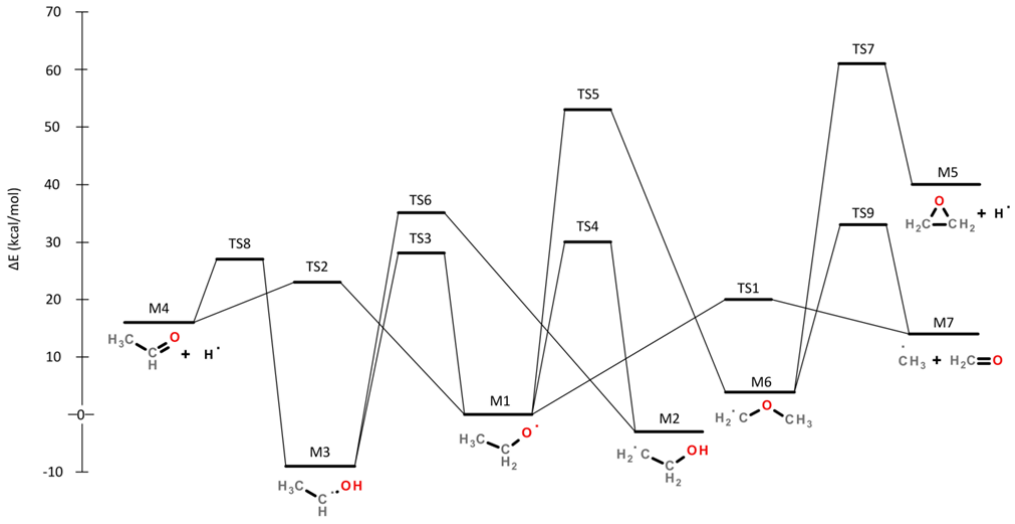

Figure 2.1: Schematic energy diagram for the possible reactions of diethyl peroxide after dissociation at M06-2X/aug-cc-pVDZ level.

Table 2.1: Molecular structure of species involved in the dissociation of diethyl peroxide

Species	Chemical structure
M1	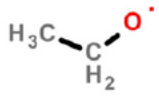
M2	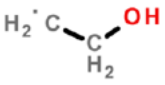
M3	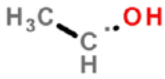
M4	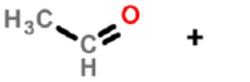
M5	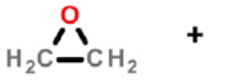
M6	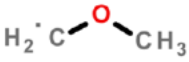
M7	

Table 2.2: Calculated energy values for possible reaction products in diethyl peroxide dissociation at the M06-2X/aug-cc-pVDZ level.

Species	E_{elec} (Ha)	ZPE (mHa)	Corrected ZPE (mHa)	BSSE (mHa)	E+ZPE+BSSE (Ha)	ΔE (mHa)	ΔE (kcal/mol)
M1	-154.312788	64.75	63.390	0	-154.249398	0	0
M2	-154.317848	65.595	64.218	0	-154.253630	-4.233	-2.7
M3	-154.328964	66.208	64.818	0	-154.264147	-14.749	-9.3
M4	-154.278004	55.685	54.516	-0.819	-154.224308	25.090	15.7
M5	-154.241648	57.983	56.765	-0.860	-154.185744	63.654	39.9
M6	-154.307578	66.042	64.655	0	-154.242923	6.475	4.1
M7	-154.280042	56.634	55.445	-2.6277	-154.227226	22.172	13.9
TS1	-154.277276	61.538	60.246	0	-154.217031	32.367	20.3
TS2	-154.269060	57.395	56.190	0	-154.212871	36.527	22.9
TS3	-154.265476	61.427	60.137	0	-154.205339	44.058	27.6

Species	E_{elec} (Ha)	ZPE (mHa)	Corrected ZPE (mHa)	BSSE (mHa)	E+ZPE+BSSE (Ha)	ΔE (mHa)	ΔE (kcal/mol)
TS4	-154.263163	62.162	60.857	0	-154.202307	47.091	29.5
TS5	-154.226204	63.272	61.943	0	-154.164261	85.137	53.4
TS6	-154.253174	61.126	59.842	0	-154.193332	56.065	35.2
TS7	-154.209832	59.517	58.267	0	-154.151565	97.833	61.4
TS8	-154.263138	57.14	55.940	0	-154.207199	42.199	26.5
TS9	-154.256892	60.598	59.325	0	-154.197567	51.830	32.5

Our calculations confirm that the experimentally determined [178] main reaction in decomposition of diethyl peroxide (eq. 2.2) have the smallest barrier height (TS1=20.3 kcal/mol).

To further investigate the effect of basis set size on our results, we also searched for TS structures and recalculated all energies using cc-pVDZ and aug-cc-pVTZ basis sets. Table 2.3 lists the relative energy of the all involved species. The differences in the calculated energies with different basis sets are shown in figure 2.2. Figure 2.3 shows correlations between the energy values calculated with cc-pVDZ↔ aug-cc-pVDZ, and aug-cc-pVDZ↔ aug-cc-pVTZ basis sets. Coefficient of determination (R-square) of fitting these data to equality line (x=y) for the former is 0.996 and for latter is 0.999.

Table 2.3: Calculated relative energy values for possible reaction products in diethyl peroxide dissociation using M06-2X functional with various basis sets.

Species	ΔE (kcal/mol)		
	cc-pVDZ	aug-cc-pVDZ	aug-cc-pVTZ
M1	0.0	0.0	0.0
M2	-0.4	-2.7	-2.5
M3	-8.1	-9.3	-9.3
M4	14.8	15.7	16.7
M5	39.6	39.9	40.6
M6	3.7	4.1	3.0
M7	11.9	13.9	13.6

Species	ΔE (kcal/mol)		
	cc-pVDZ	aug-cc-pVDZ	aug-cc-pVTZ
TS1	21.1	20.3	19.3
TS2	22.6	22.9	23.5
TS3	28.7	27.6	27.7
TS4	30.1	29.5	30.2
TS5	54.6	53.4	52.6
TS6	37.6	35.2	35.8
TS7	61.2	61.4	61.7
TS8	26.1	26.5	26.8
TS9	32.3	32.5	31.4

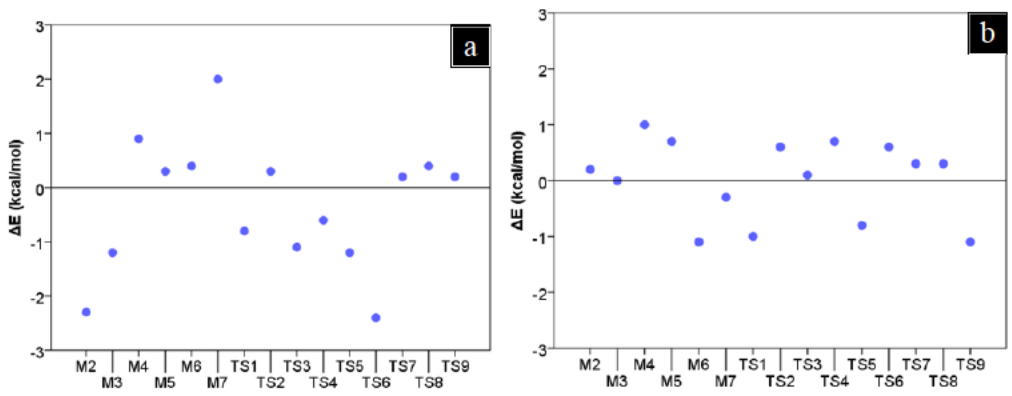

Figure 2.2: Change in the calculated energy of involved species using M06-2X functional by increasing size of basis set from a) cc-pVDZ to aug-cc-pVDZ, and b) aug-cc-pVDZ to aug-cc-pVTZ.

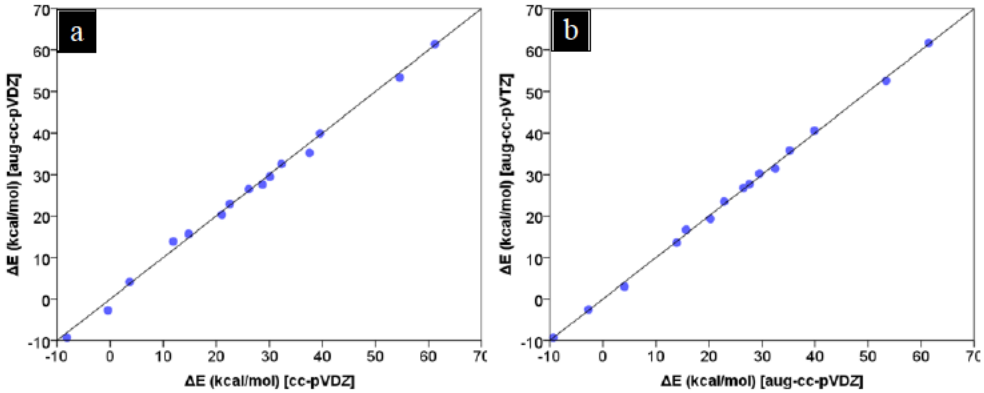

Figure 2.3: Correlations between the calculated energies with a) M06-2X/cc-pVDZ↔M06-2X/aug-cc-pVDZ, and b) M06-2X/aug-cc-pVDZ↔M06-2X/aug-cc-pVTZ

These results show that using basis sets bigger than aug-cc-pVDZ will not have any meaningful influence on our calculated energy values. Thus, the rest of our calculations are done at M06-2X/aug-cc-pVDZ level unless stated otherwise.

To ensure sufficient accuracy of our DFT calculations, we compared our calculated uncorrected relative energy values from M06-2X/aug-cc-pVDZ method with the energies calculated from coupled cluster single double and perturbative triple, CCSD(T) [181], method for the geometry optimized by DFT method using the same basis set. The results of calculated energy differences with M06-2X and CCSD(T) methods are listed in table 2.4. Correlation between these values has been also graphically represented in figure 2.4.

Table 2.4: Calculated uncorrected relative energy values for possible reaction products in diethyl peroxide dissociation at M06-2X/aug-cc-pVDZ and CCSD(T)/aug-cc-pVDZ level.

Species	ΔE (kcal/mol)	
	M06-2X	CCSD(T)
M1	0.0	0.0
M2	-3.2	-2.3
M3	-10.2	-8.5
M4	21.8	20.7
M5	44.6	48.9
M6	3.3	5.1
M7	20.5	15.8
TS1	22.3	20.1
TS2	27.4	26.8
TS3	29.7	31.5
TS4	31.1	31.4
TS5	54.3	55.0
TS6	37.4	40.7
TS7	64.6	69.2
TS8	31.2	31.2
TS9	35.1	32.6

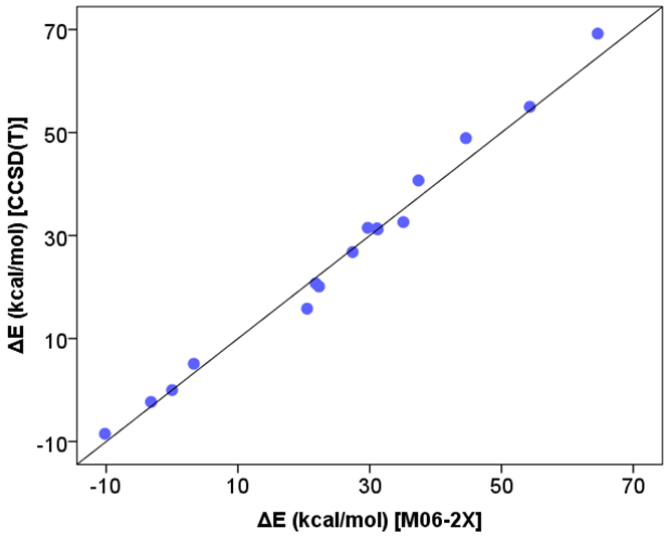

Figure 2.4: Correlation between the relative uncorrected energy of radicals and transition states in diethyl peroxide dissociation at M06-2X/aug-cc-pVDZ and CCSD(T)/aug-cc-pVDZ levels.

By comparing the calculated relative energy values we can safely conclude that calculations at M06-2X/aug-cc-pVDZ level are sufficiently accurate to investigate the main reactions in this system and higher level calculations (i.e CCSD(T)) are not providing any additional information.

Activation energy of all reactions in forward and backwards direction based on the located transition states are listed in table 2.5. Reactions are numbered according to their respective TS.

Table 2.5: Activation energies of the possible reactions of diethyl peroxide after dissociation at M06-2X/aug-cc-pVDZ level.

Reactant		TS	Product		Activation energy (kcal/mol)	
					Forward reaction	Backwards reaction
M1	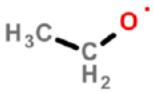	TS1		M7	20.3	6.4
M1	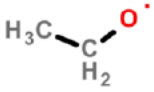	TS2	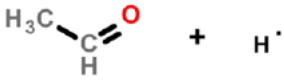	M4	22.9	7.2
M1	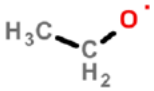	TS3	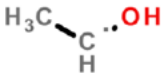	M3	27.6	36.9
M1	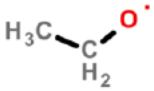	TS4	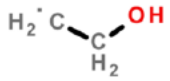	M2	29.5	32.2
M1	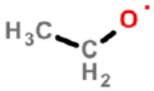	TS5	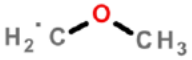	M6	53.4	49.3
M3	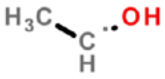	TS6	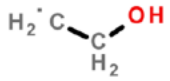	M2	44.5	37.9
M6	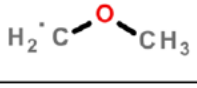	TS7	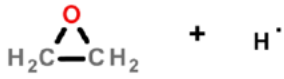	M5	57.3	21.5
M3	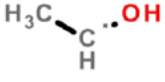	TS8	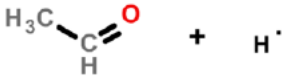	M4	35.8	10.8
M6		TS9		M7	28.4	18.6

Reactions 1-5 (corresponding to TS 1-5, respectively) can convert ethyloxidanyl into different products. Thermal decomposition of peroxides is a thermally active

reaction. We can use Arrhenius equation to estimate relative rate constant of each involved reaction:

$$k = Ae^{\frac{-E_a}{RT}} \quad (2.6)$$

where, k is rate constant, A is frequency factor or pre-exponential factor, E_a is activation energy, R is universal gas constant (1.9872041×10^{-3} kcal.K^{-1}.mol^{-1}) and T is absolute temperature. We consider the T to be the room temperature (298 K). The factor A may be interpreted as the limiting specific rate for molecules of very high energy which in our case, all of these unimolecular reactions have common reactant; therefore to have a rough estimation for comparisons purpose we assume it to be the same for all these five reactions. Thus, rate constants for these reactions are:

$k_1=A\times1.2957\times10^{-15}$ (2.7)

$k_2=A\times1.6060\times10^{-17}$ (2.8)

$k_3=A\times5.7395\times10^{-21}$ (2.9)

$k_4=A\times2.3199\times10^{-22}$ (2.10)

$k_5=A\times6.8837\times10^{-40}$ (2.11)

Unimolecular dissociation reactions are generally considered as first-order reactions. By comparing the rate constants, we see that reaction 1 (methyl radical abstraction) is the fastest reaction. By comparison, reactions 2-5 are slower. Thus, most of ethyloxidanyl radicals are dissociated with methyl radical abstraction which is in agreement with experimental findings describing it as the main decomposition mechanism [178].

Difference in absorption spectra of diethyl peroxide with various radicals in visible region is shown in figure 2.5. Our calculations show that first electronic excitation in diethyl peroxide occurs at around 230nm and there is no transition in visible range. Thus, our differential absorption plot will only show absorptions of produced radicals in dissociation process. As it can be seen, only 3 radicals (M1, M3, and M6) have absorption (more specifically, absorption tails) in this region. Calculated excitation

lowest energies and the most intense absorption among the first 20 transitions for each radical are listed in table 2.6.

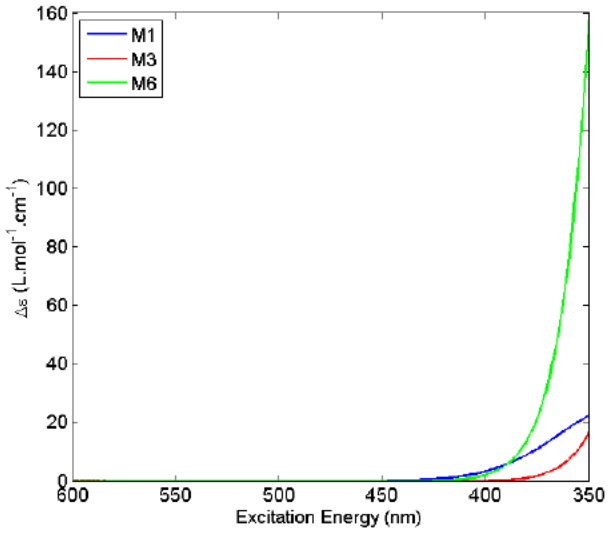

Figure 2.5: Difference in absorption spectra of diethyl peroxide with various radicals in visible region.

Table 2.6: Calculated excitation energies with the lowest energy, and the highest oscillator strength for radicals involved in dissociation of diethyl peroxide at M06-2X/aug-cc-pVDZ level.

Species	Lowest Energy excitation		Highest intensity excitation	
	λ (nm)	Oscillator strength	λ (nm)	Oscillator strength
M1	338.05	0.0006	211.64	0.0284
M2	255.74	0.0043	245.36	0.0233
M3	297.65	0.0045	167.70	0.0440
M4	180.62	0.0151	135.14	0.1721
M5	166.90	0.0133	128.50	0.0795
M6	303.19	0.0261	208.40	0.0545
M7	236.52	0.0366	128.43	0.1475

We did all our calculations in gas phase. But, most of the experiments are commonly done in the presence of solvents. To estimate the effects of solvents on the

calculated excitation energies of each radical, we optimized the geometry and calculated the excitation energies of the species involved in the first reactions of dissociation products in acetonitrile (CH_3-C≡N) and ethanol (CH_3-CH_2-OH) which are the two commonly used solvents. Dielectric constants of acetonitrile and ethanol are taken as 35.688 and 24.852, respectively which correspond to room temperature experimental values [182; 183]. The shifts in the energy of the important low energy excitation peaks of initial radical and first reaction products are listed in table 2.7. Changes in absorption spectrum of M3 upon solvation as a typical behavior in these solvents are shown in figure 2.6.

Table 2.7: Shift in the excitation energy of diethyl peroxide dissociation radicals upon solvation in acetonitrile and ethanol.

Species	Excitation peak position (nm)	Excitation peak shift (nm)	
		In acetonitrile	In ethanol
M1	211	+15	+14
M2	246	-2	-2
M3	262	-5	-5
M4	164	-4	-4
M6	303	-7	-6
M7	237	-3	-3

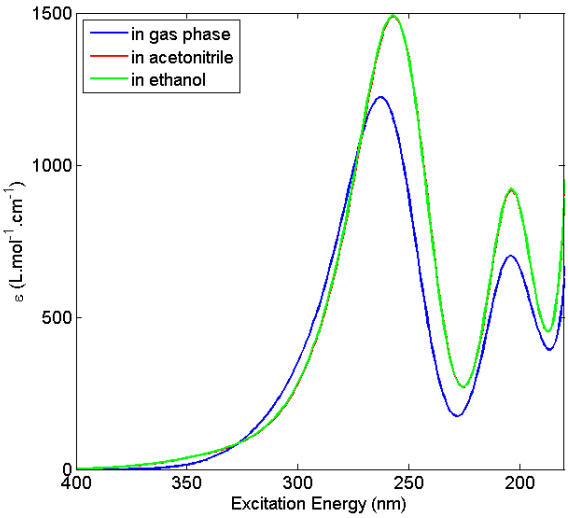

Figure 2.6: Computed absorption spectra for M3 (CH_3˙CHOH radical) in gas phase, acetonitrile and ethanol.

As it can be seen in table 2.7 and figure 2.6, TDDFT/PCM calculation for radicals in both acetonitrile and ethanol show similar shift in excitation energies. Despite changes in the intensity of the absorption peaks which is not much helpful for characterization of radicals, the amount of change in excitation energy is negligible in comparison with our calculations accuracy.

2.2 Di-tert-butyl peroxide

We chose di-tert-butyl peroxide as the next molecule for study. Experiments show [184] that the main reactions in decomposition of di-tert-butyl peroxide are:

$$(CH_3)_3COOC(CH_3)_3 \rightarrow 2(CH_3)_3CO^{\cdot} \quad (2.12)$$

$$(CH_3)_3CO^{\cdot} \rightarrow {}^{\cdot}CH_3 + (CH_3)_2C{=}O \quad (2.13)$$

Staring from tert-butyloxidanyl radical ($(CH_3)_3CO^{\cdot}$), we followed the same process as for diethyl peroxide and tried to identify the possible products and activation energy of each reaction based on their respective TS energies. Figure 2.7 shows schematic

energy diagram for the identified possible reactions in this system. Chemical structures of the all involved species are listed in table 2.8. Table 2.9 lists the corrected relative energy of the all involved species at M06-2X/aug-cc-pVDZ level. It must be noted that by increasing the number of atoms in molecule, the number of molecule's degree of freedom is increasing and consequently the number of PES's dimensions are increasing which makes it harder to map all characteristic stationary points on PES to reaction coordinates. Moreover, similarities in the geometries of different TSs make it harder to successfully locate them. Therefore, we try to limit our investigations on larger molecules mostly to the reactions with low activation energies.

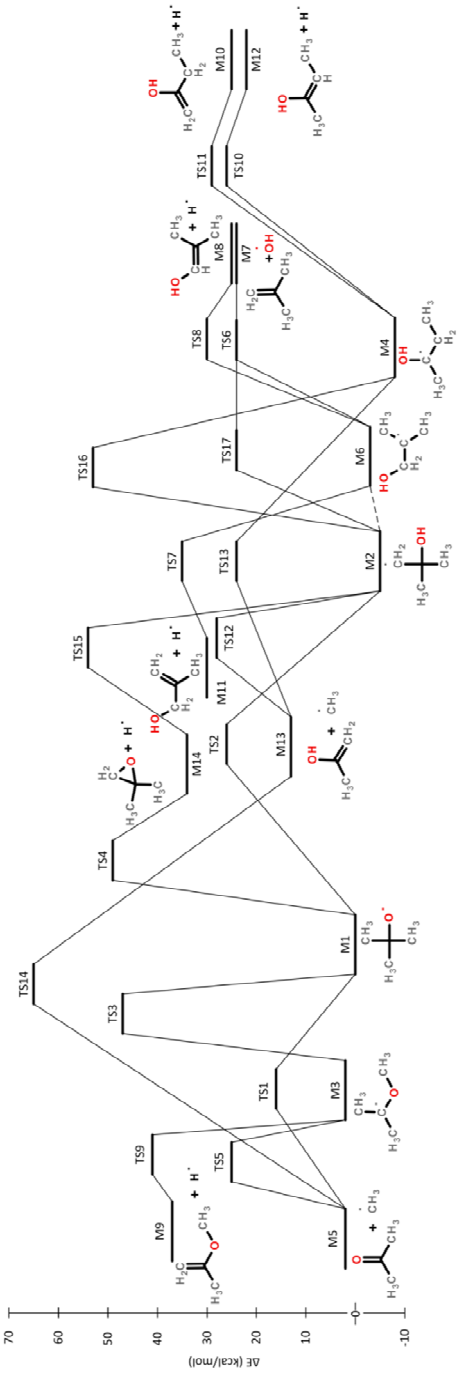

Figure 2.7: Schematic energy diagram for the possible reactions of di-tert-butyl peroxide after dissociation at M06-2X/aug-cc-pVDZ level.

Table 2.8: Molecular structure of species involved in the dissociation of di-tert-butyl peroxide.

Species	Chemical structure
M1	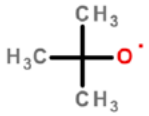
M2	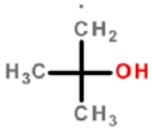
M3	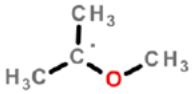
M4	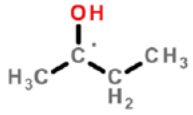
M5	
M6	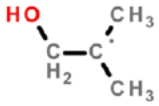
M7	
M8	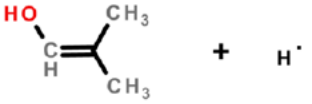
M9	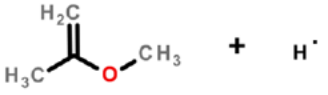
M10	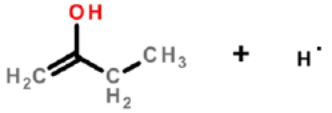

Species	Chemical structure
M11	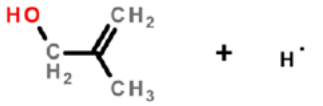
M12	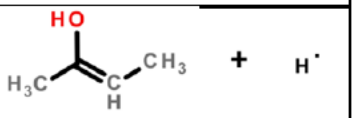
M13	
M14	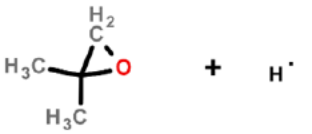

Table 2.9: Calculated energy values for possible reaction products in di-tert-butyl peroxide dissociation using M06-2X functional with aug-cc-pVDZ basis set.

Species	ΔE (kcal/mol)
M1	0.0
M2	-4.6
M3	2.4
M4	-7.9
M5	2.2
M6	-2.8
M7	24.2
M8	25.2
M9	36.6
M10	24.8
M11	30.4
M12	22.3
M13	12.7
M14	33.8
TS1	15.7
TS2	26.4
TS3	47.0

Species	ΔE (kcal/mol)
TS4	48.8
TS5	25.1
TS6	23.6
TS7	34.6
TS8	29.8
TS9	41.0
TS10	25.8
TS11	29.2
TS12	27.8
TS13	23.5
TS14	65.3
TS15	53.7
TS16	52.6
TS17	23.7

Relative uncorrected electronic energy of involved species at M06-2X/aug-cc-pVDZ and CCSD(T)/aug-cc-pVDZ level are listed in table 2.10. Correlation between the calculated values is also graphically represented in figure 2.8.

Table 2.10: Calculated uncorrected relative energy values for possible reaction products in di-tert-butyl peroxide dissociation at M06-2X/aug-cc-pVDZ and CCSD(T)/aug-cc-pVDZ levels.

Species	ΔE (kcal/mol)	
	M06-2X	CCSD(T)
M1	0.0	0.0
M2	-3.7	-2.6
M3	2.2	5.7
M4	-8.4	-5.7
M5	11.3	9.6
M6	-2.6	0.2
M7	30.6	28.1
M8	32.9	36.3
M9	44.8	48.5
M10	32.9	35.9
M11	37.7	40.2
M12	30.8	34.3
M13	20.8	21.7
M14	42.2	46.8
TS1	18.3	17.3
TS2	29.4	29.7
TS3	49.0	50.5
TS4	53.1	56.3
TS5	28.6	28.3
TS6	25.8	23.7
TS7	39.5	41.5
TS8	34.8	37.9
TS9	46.0	49.4
TS10	30.6	34.1
TS11	34.1	36.7
TS12	30.8	30.7
TS13	26.4	27.4
TS14	77.8	78.9
TS15	58.6	61.3
TS16	55.3	59.1

Species	ΔE (kcal/mol)	
	M06-2X	CCSD(T)
TS17	25.8	22.9

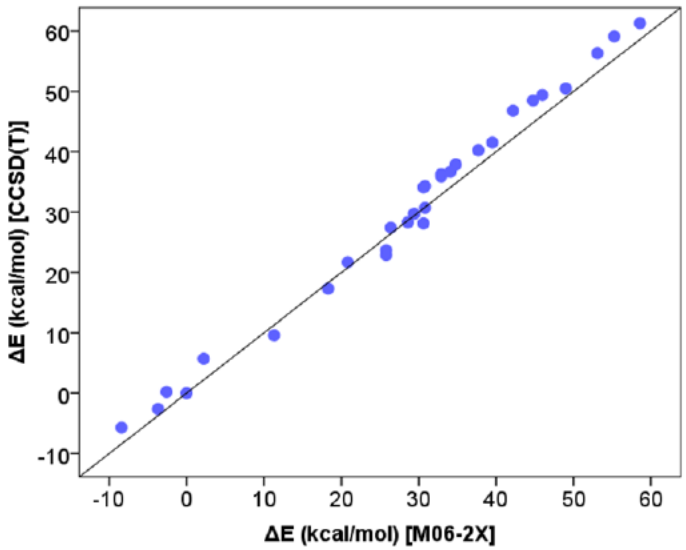

Figure 2.8: Correlation between the relative uncorrected energy of radicals and transition states in diethyl peroxide dissociation at M06-2X/aug-cc-pVDZ and CCSD(T)/aug-cc-pVDZ levels.

As it can be seen in table 2.10 and figure 2.8, in this case also M06-2X/aug-cc-pvDZ level energy calculations are sufficient and higher level (CCSD(T)) energies do not provide any additional information. Activation energy of all reactions in forward and backwards direction based on the located transition states are listed in table 2.11.

Table 2.11: Activation energies of the possible reactions of di-tert-butyl peroxide after dissociation at M06-2X/aug-cc-pVDZ level.

Reactant		TS	Product		Activation energy (kcal/mol)	
					Forward reaction	Backwards reaction
M1	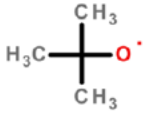	1	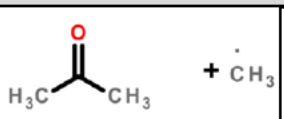	M5	15.7	13.5
M1	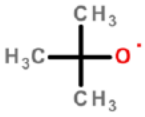	2	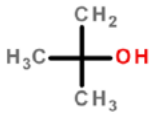	M2	26.4	31.0
M1	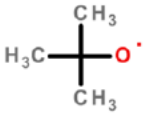	3	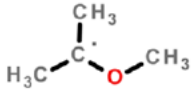	M3	47.0	44.6
M1	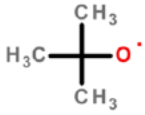	4	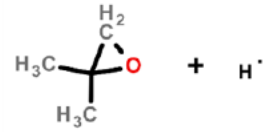	M14	48.8	15.0
M3	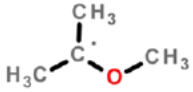	5	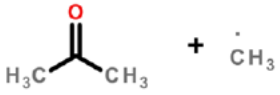	M5	22.7	22.9
M6	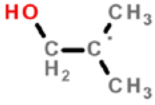	6	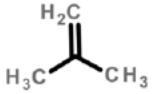	M7	26.4	-0.6
M6	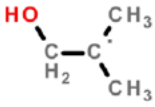	7	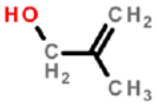	M11	37.4	4.2
M6	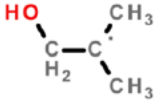	8	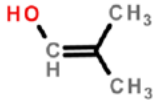	M8	32.6	4.6
M3	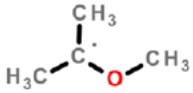	9	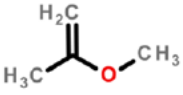	M9	38.6	4.4

Reactant		TS	Product		Activation energy (kcal/mol)	
					Forward reaction	Backwards reaction
M4	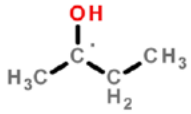	10	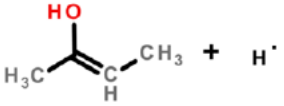	M12	33.7	3.5
M4	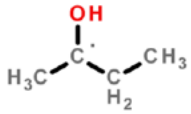	11	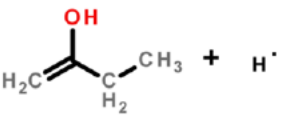	M10	37.1	4.4
M2	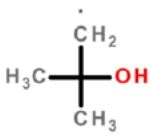	12	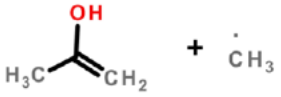	M13	32.4	15.1
M4	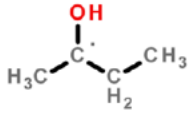	13	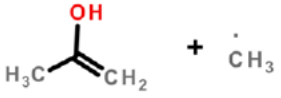	M13	31.4	10.8
M5	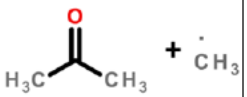	14	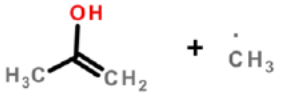	M13	63.1	52.6
M2	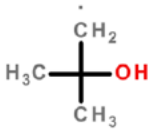	15	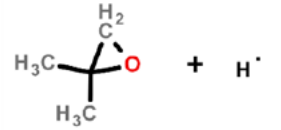	M14	58.3	19.9
M2	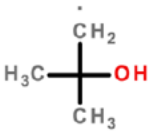	16	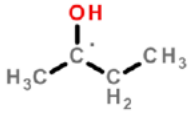	M4	57.2	60.5
M2	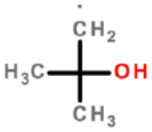	17	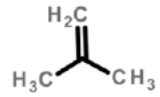	M7	28.3	-0.5

As it can be seen in table 2.11, we found negative value for activation energy of OH addition to isobutene (reactions 6 and 17). This is in agreement with literature which found that all the activation energies for alkenes + ˙OH reactions are close to -1

kcal/mol [185]. It's been found out that these reactions are not elemental, and "they consists of a reversible first step involving the formation of a pre-reactive complex, followed by the irreversible formation of an addition adduct" [186]. Our transition state is the first transition state in the reaction which have negative energy difference with respect to the reactants [187]. The resulted values are in the error range of our calculation method and these reactions for characterization purpose can be practically treated as transition-less reactions.

Reactions 1-4 can convert tert-butyloxidanyl into different radicals. Using Arrhenius equation to estimate relative rate constant of each reaction at room temperature with the same assumptions as the former section, we get:

$$k_1 = A \times 3.0622 \times 10^{-12} \quad (2.14)$$

$$k_2 = A \times 4.3544 \times 10^{-20} \quad (2.15)$$

$$k_3 = A \times 3.3995 \times 10^{-35} \quad (2.16)$$

$$k_4 = A \times 1.6268 \times 10^{-36} \quad (2.17)$$

By comparing the rate constants, we see that reaction 1 (methyl radical abstraction) is the fastest reaction. By comparison, reactions 2, 3, and 4 are much slower. Thus, majority of tert-butyloxidanyl radicals at room temperature are dissociated with methyl radical abstraction which is in agreement with experimental findings describing it as the main decomposition mechanism [184].

Difference in absorption spectra of di-tert-butyl peroxide with various radicals in visible region is shown in figure 2.9. Our calculations show that first electronic excitation in di-tert-butyl peroxide occurs at around 190nm and there is no transition in visible range. Thus, our differential absorption plot will only show absorptions of produced radicals in dissociation process. As it can be seen, only 5 radicals (M1, M3, M4, M6, and M7) have absorption in this region. Calculated energy of the first and also the most intense absorption among the first 20 transitions for each radical are listed in table 2.12.

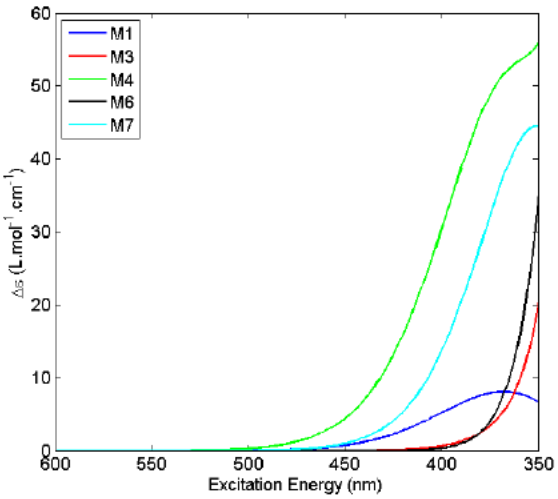

Figure 2.9: Difference in absorption spectra of di-tert-butyl peroxide with various radicals in visible region.

Table 2.12: Calculated excitation energies with the lowest energy, and the highest oscillator strength for radicals involved in dissociation of di-tert-butyl peroxide at M06-2X/aug-cc-pVDZ level

Species	Lowest Energy excitation		Highest intensity excitation	
	λ (nm)	Oscillator strength	λ (nm)	Oscillator strength
M1	368.54	0.0002	167.94	0.0293
M2	259.81	0.0017	174.92	0.0390
M3	331.52	0.0002	276.08	0.0350
M4	368.00	0.0012	230.13	0.0180
M5	236.53	0.0366	137.30	0.2494
M6	300.31	0.0073	253.63	0.0259
M7	350.67	0.0011	186.23	0.2233
M8	223.13	0.0002	169.39	0.2530
M9	221.34	0.0203	199.51	0.1486
M10	228.92	0.0118	179.97	0.1200
M11	203.71	0.0013	186.23	0.2024

Species	Lowest Energy excitation		Highest intensity excitation	
	λ (nm)	Oscillator strength	λ (nm)	Oscillator strength
M12	217.29	0.0066	176.68	0.1768
M13	230.61	0.0062	194.85	0.1885
M14	170.91	0.0012	134.00	0.0639

The shifts in the energy of the important low energy excitation peaks of initial radical and first reaction products upon solvation in acetonitrile and ethanol are listed in table 2.13.

Table 2.13: Shift in the excitation energy of di-tert-butyl peroxide dissociation radicals upon solvation in acetonitrile and ethanol.

Species	Excitation peak position (nm)	Excitation peak shift (nm)	
		In acetonitrile	In ethanol
M1	234	+16	+15
M2	245	-3	-3
M3	276	-7	-7
M5	237	-4	-3
M14	156	+1	+1

As it can be seen in table 2.13, also in case of radicals involved in the dissociation of di-tert-butyl peroxide, TDDFT/PCM calculations are not showing large changes in the position of absorption peaks.

2.3 Dicumyl peroxide

Photochemical decomposition of dicumyl peroxide and cumene hydroperoxide have been the subject of various studies in the past [188] which both of them result in cumyloxy radical.

Studies of the decomposition of cumene hydroperoxide had shown that the cumyloxy radical decompose to acetophenone and a methyl radical (eq. 2.18) or convert to 2-phenyl-2-propanol (eq. 2.19) [189]:

$$C_6H_5\text{-}C(CH_3)_2\text{-}O^{\cdot} \rightarrow C_6H_5\text{-}C(CH_3)\,O + {}^{\cdot}CH_3 \qquad (2.18)$$

$$C_6H_5\text{-}C(CH_3)_2\text{-}O^{\cdot} + R\text{-}H \rightarrow C_6H_5\text{-}C(CH_3)\,OH + R^{\cdot} \qquad (2.19)$$

In absence of hydrogen donors, methyl radical abstraction reaction (eq. 2.18) is the dominant decomposition mechanism.

Although "instantaneous" increase in visible range absorption have been observed in photochemical decomposition of cumyloxyl radicals [190], yet no satisfactory explanation have been provided for this phenomenon. Recent studies showed that a large number of reactions can be involved in thermal decomposition of dicumyl peroxide in various reaction conditions (i.e. solvent, presence of oxygen, etc.) [191] which is a serious obstacle in interpretation of experimental results. Schematic energy diagram for the possible initial reactions starting from M1 are shown in figure 2.10. Figures 2.11 and 2.12 show a more complete map of studied region on PES. Chemical structures of the all involved species are listed in table 2.14.

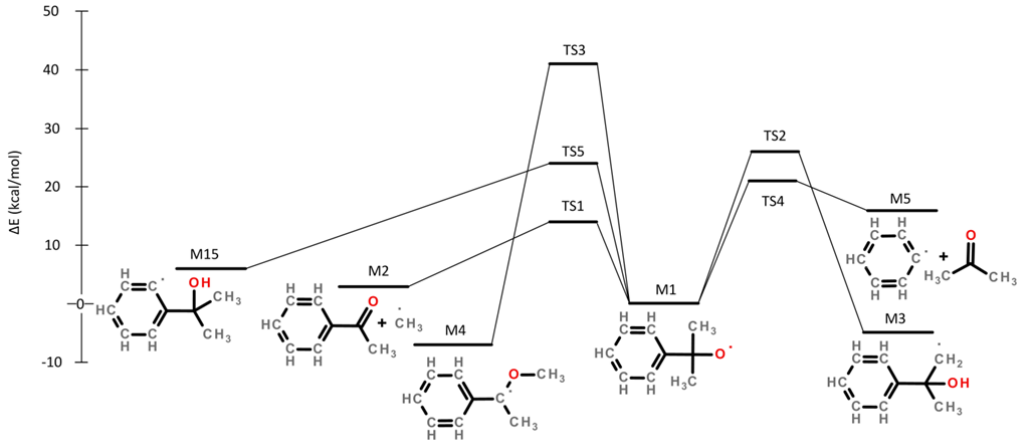

Figure 2.10: Schematic energy diagram for the possible initial reactions of dicumyl peroxide after dissociation at M06-2X/aug-cc-pVDZ level.

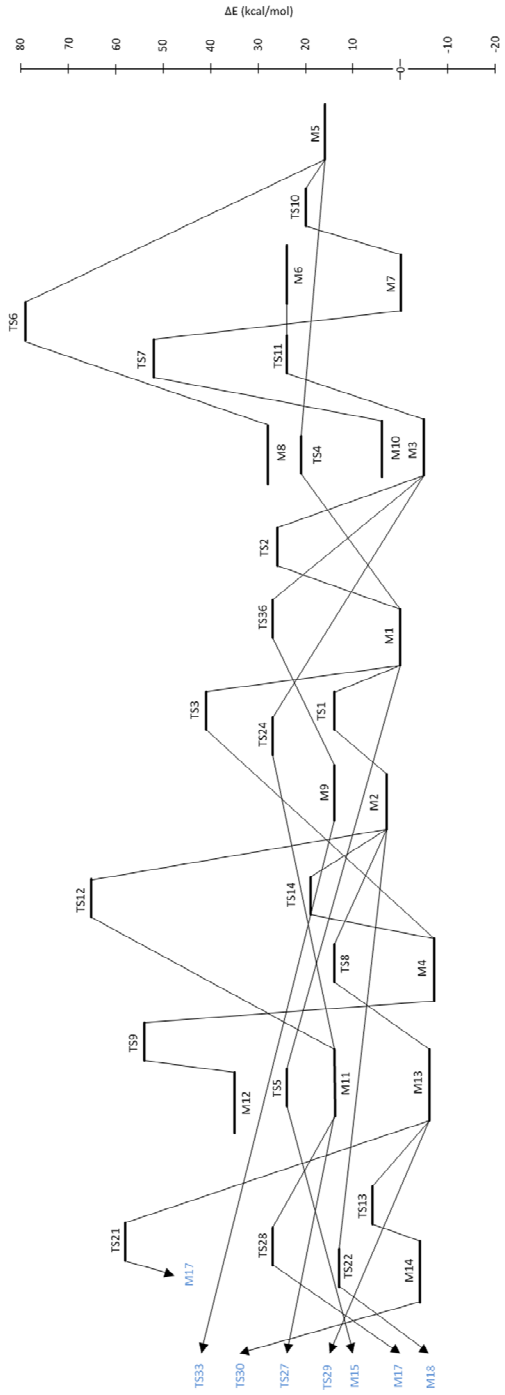

Figure 2.11: Schematic energy diagram for the possible reactions of dicumyl peroxide after dissociation at M06-2X/aug-cc-pVDZ level (part I)

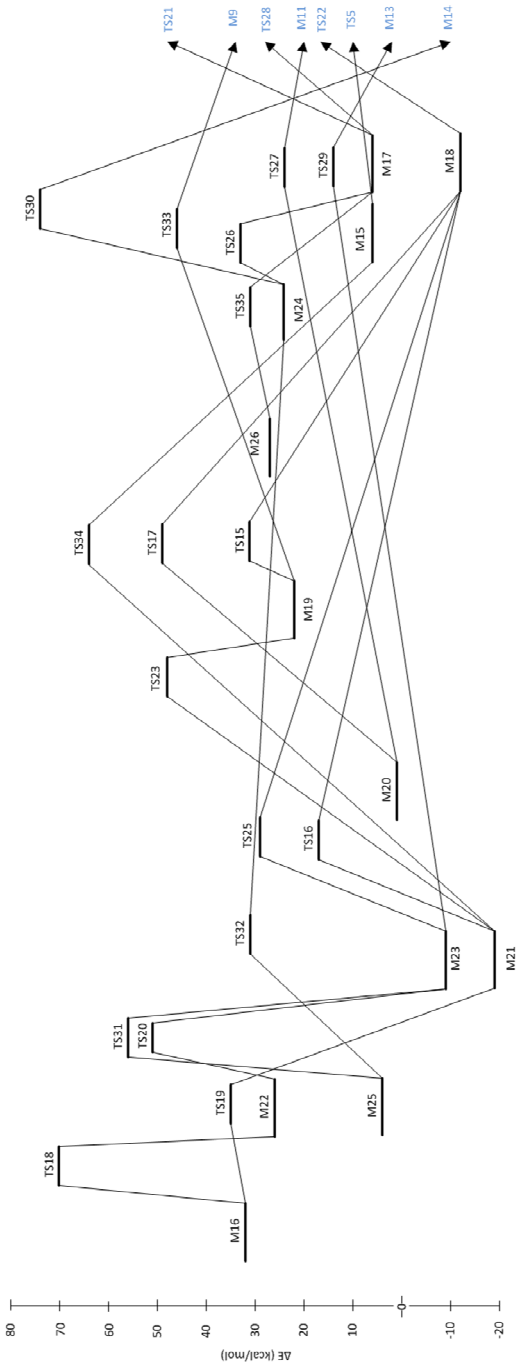

Figure 2.12: Schematic energy diagram for the possible reactions of dicumyl peroxide after dissociation at M06-2X/aug-cc-pVDZ level (part II)

Table 2.14: Molecular structure of species involved in the dissociation of dicumyl peroxide.

Species	Chemical structure
M1	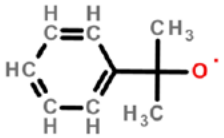
M2	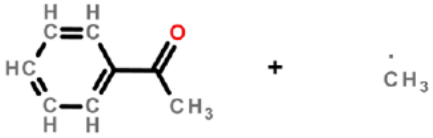
M3	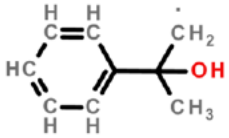
M4	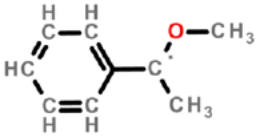
M5	
M6	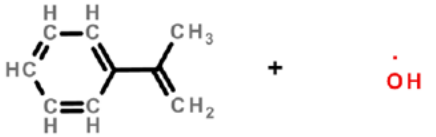
M7	
M8	

Species	Chemical structure
M9	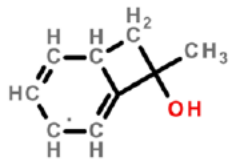
M10	
M11	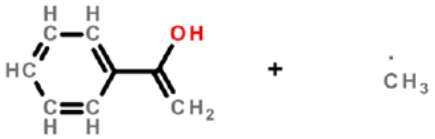
M12	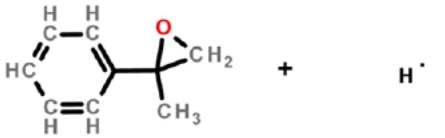
M13	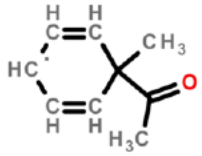
M14	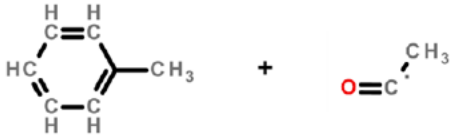
M15	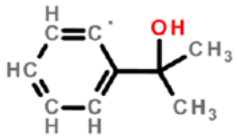
M16	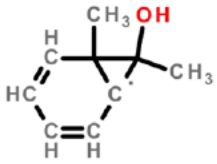

Species	Chemical structure
M17	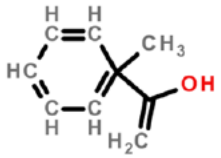
M18	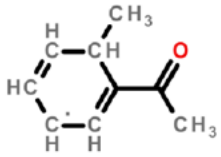
M19	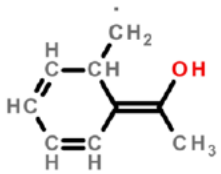
M20	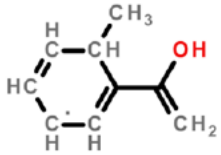
M21	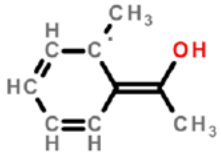
M22	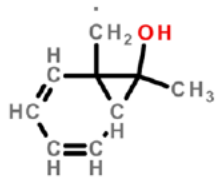
M23	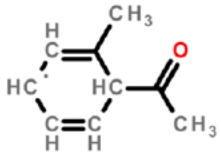

Species	Chemical structure
M24	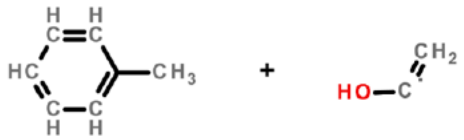
M25	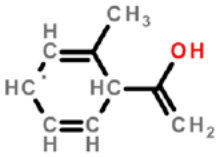
M26	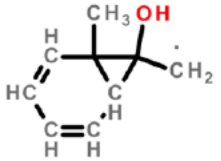

Calculated energy values for possible reaction products in dicumyl peroxide dissociation are listed in table 2.15. Activation energies of the possible reactions are listed in table 2.16.

Table 2.15: Calculated energy values for possible reaction products in dicumyl peroxide dissociation using M06-2X functional with aug-cc-pVDZ basis set.

Species	ΔE (kcal/mol)	Species	ΔE (kcal/mol)
TS1	13.7	M1	0.0
TS2	26.0	M2	3.0
TS3	40.9	M3	-4.5
TS4	20.8	M4	-7.1
TS5	24.4	M5	16.0
TS6	79.1	M6	23.9
TS7	52.2	M7	-0.1
TS8	14.4	M8	28.0
TS9	53.5	M9	14.2
TS10	19.9	M10	4.1
TS11	23.9	M11	14.4
TS12	64.8	M12	35.3
TS13	6.1	M13	-6.3
TS14	18.8	M14	-4.1
TS15	30.6	M15	5.6
TS16	16.6	M16	31.5
TS17	48.8	M17	6.2
TS18	70.3	M18	-11.8
TS19	35.4	M19	22.2
TS20	51.2	M20	1.3
TS21	58.3	M21	-18.6
TS22	13.0	M22	26.0
TS23	48.3	M23	-8.6
TS24	26.6	M24	24.3
TS25	28.9	M25	3.6
TS26	32.8	M26	27.2
TS27	24.2		
TS28	26.7		
TS29	13.5		
TS30	74.0		
TS31	56.2		
TS32	30.9		
TS33	45.6		
TS34	64.4		
TS35	30.8		
TS36	27.4		

Table 2.16: Activation energies of the possible reactions of dicumyl peroxide after dissociation at M06-2X/aug-cc-pVDZ level.

Reactant		TS	Product		Activation energy (kcal/mol)	
					Forward reaction	Backwards reaction
M1	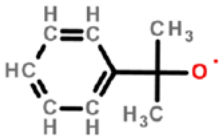	TS1	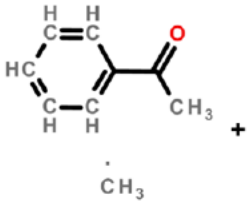	M2	13.7	10.7
M1	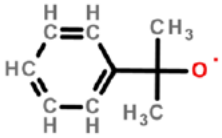	TS2	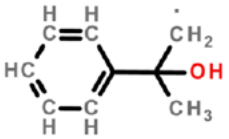	M3	26.0	30.5
M1	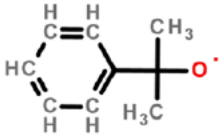	TS3	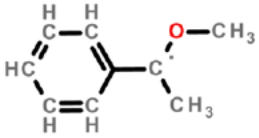	M4	40.9	48.0
M1	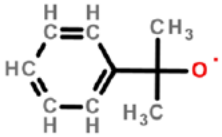	TS4	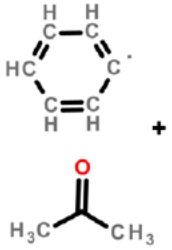	M5	20.8	4.8
M1	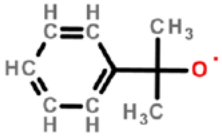	TS5	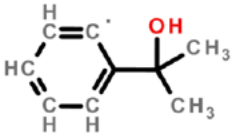	M15	24.4	18.8

Reactant		TS	Product		Activation energy (kcal/mol)	
					Forward reaction	Backwards reaction
M5	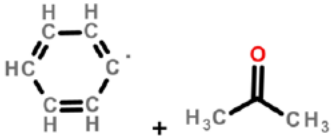	TS6	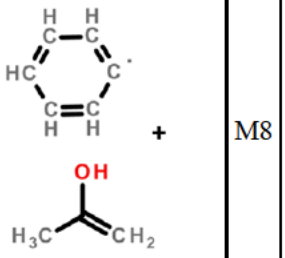	M8	63.1	51.1
M7	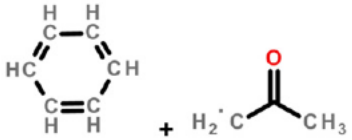	TS7	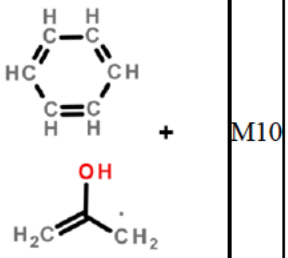	M10	52.3	48.1
M2	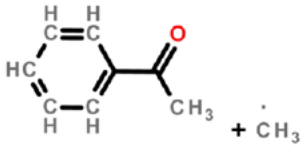	TS8	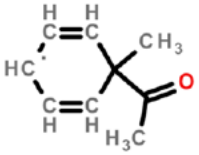	M13	11.4	20.7
M4	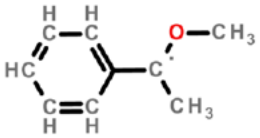	TS9	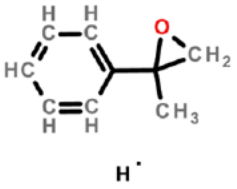	M12	60.6	18.2
M5	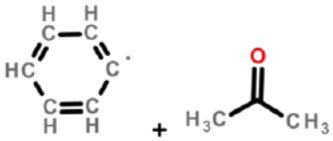	TS10	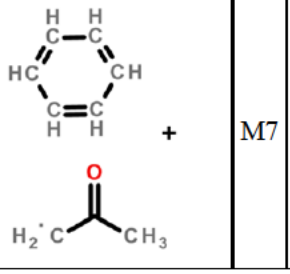	M7	3.9	20.0

Reactant		TS	Product		Activation energy (kcal/mol)	
					Forward reaction	Backwards reaction
M3	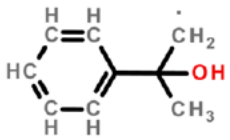	TS11	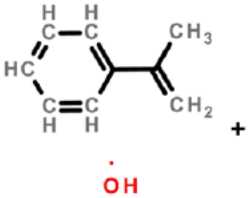	M6	28.4	0
M2	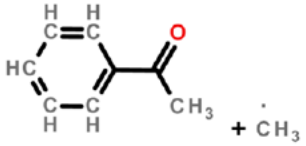	TS12	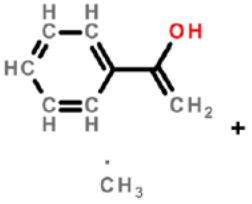	M11	61.8	50.4
M13	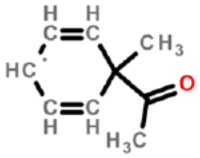	TS13	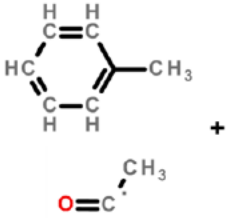	M14	12.4	10.2
M2	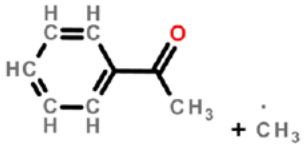	TS14	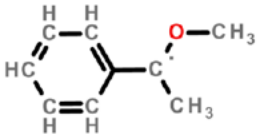	M4	15.8	25.9
M18	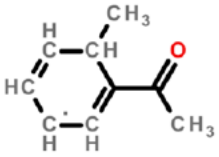	TS15	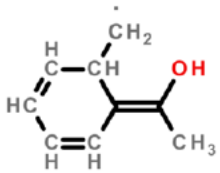	M19	42.4	8.4
M18	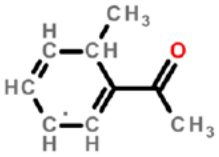	TS16	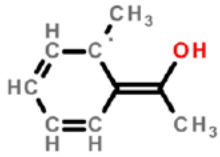	M21	28.4	35.2

Reactant		TS	Product		Activation energy (kcal/mol)	
					Forward reaction	Backwards reaction
M18	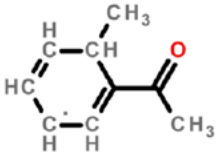	TS17	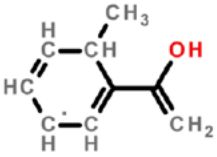	M20	60.6	47.5
M22	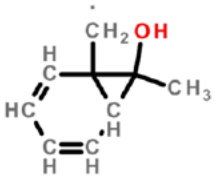	TS18	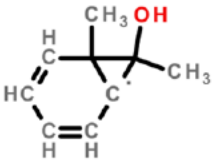	M16	44.3	38.8
M21	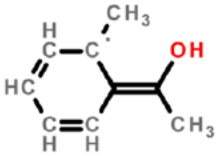	TS19	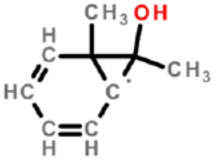	M16	54.0	3.9
M23	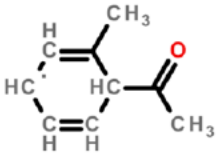	TS20	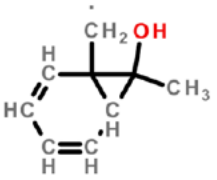	M22	59.8	25.2
M13	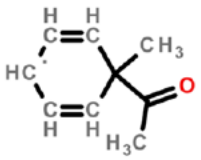	TS21	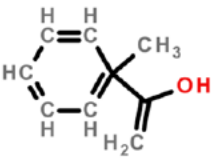	M17	64.6	52.1
M2	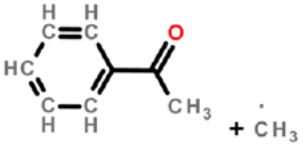	TS22	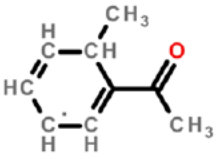	M18	10.0	24.8

Reactant		TS	Product		Activation energy (kcal/mol)	
					Forward reaction	Backwards reaction
M19	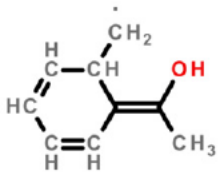	TS23	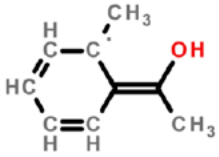	M21	26.1	66.9
M3	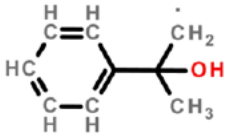	TS24	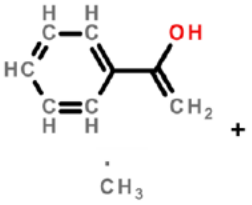	M11	31.1	12.2
M18	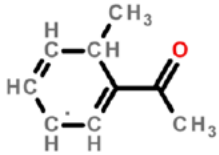	TS25	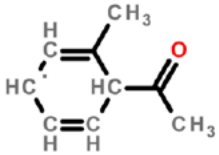	M23	40.7	37.5
M17	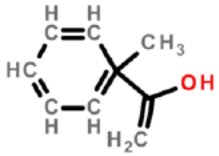	TS26	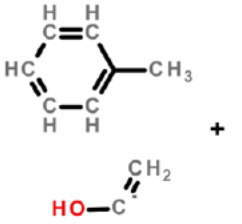	M24	26.6	8.5
M11	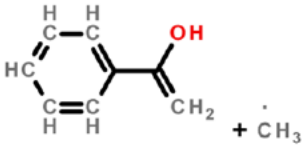	TS27	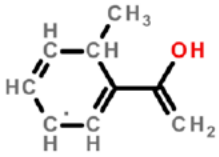	M20	9.8	22.9
M11	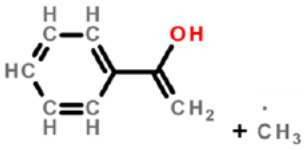	TS28	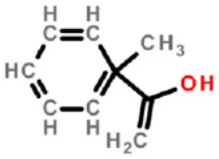	M17	12.3	20.5

Reactant		TS	Product		Activation energy (kcal/mol)	
					Forward reaction	Backwards reaction
M13	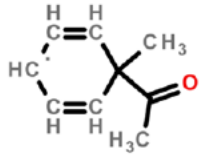	TS29	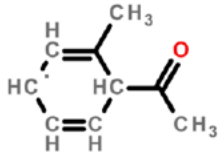	M23	19.8	22.1
M14	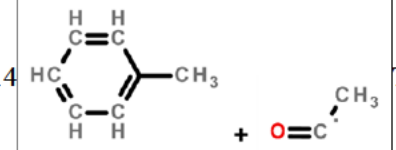	TS30	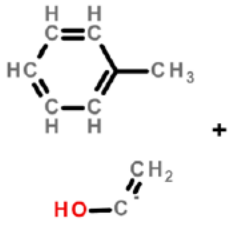	M24	78.1	49.7
M23	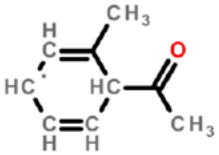	TS31	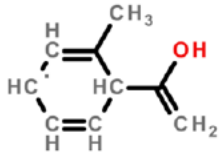	M25	64.8	52.6
M25	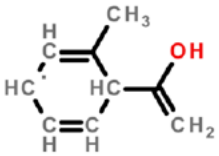	TS32	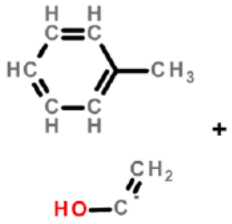	M24	27.3	6.6
M19	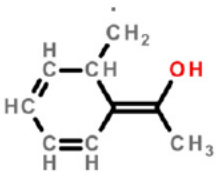	TS33	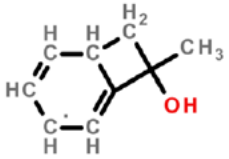	M9	23.4	31.4
M21	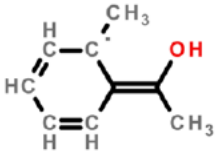	TS34	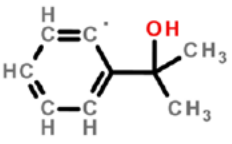	M15	83.0	58.8

Reactant		TS	Product		Activation energy (kcal/mol)	
					Forward reaction	Backwards reaction
M26	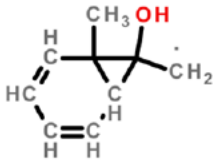	TS35	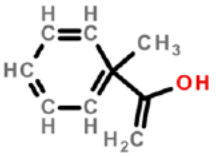	M17	3.6	24.6
M3	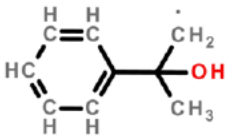	TS36	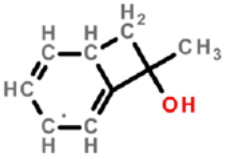	M9	31.9	13.2

Also in case of dicumyl peroxide decomposition we found zero value for activation energy of ˙OH addition to α-methylstyrene (reaction 11) which its reason has been discussed before.

Difference in absorption spectra of dicumyl peroxide with various radicals in visible region is shown in figure 2.13. Our calculations show that first electronic excitation in dicumyl peroxide occurs at around 234nm and there is no transition in visible range. Thus, our differential absorption plot will only show absorptions of produced radicals in dissociation process. Despite limited availability of experimental data of absorption spectra of radicals, there are some experiments which show visible absorption for CH3˙CO (M14) [192] as our calculations indicates. Although the goal of our investigation was not to locate all minima on PES, but as it can be seen, there are many species which show absorption in visible range. This makes interpretation of time-resolved UV-Vis absorption observations in this system difficult.

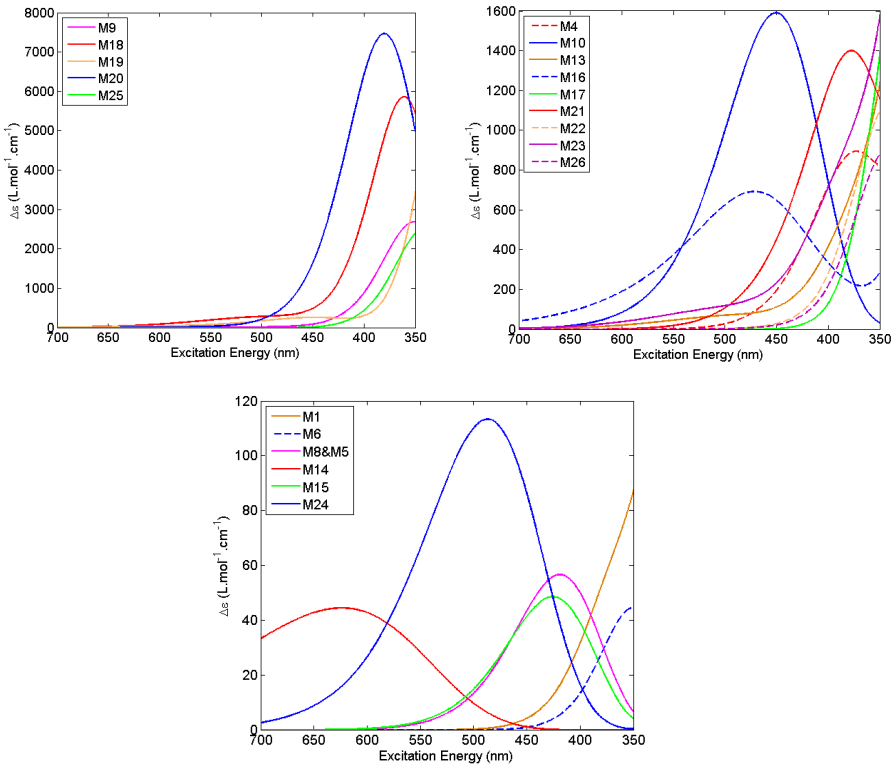

Figure 2.13: Difference in absorption spectra of dicumyl peroxide with various radicals in visible region.

Calculated energy of the first, and also the most intense absorptions among the first 20 transition for each radical are listed in table 2.17.

Table 2.17: Calculated excitation energies with the lowest energy, and the highest oscillator strength for radicals involved in dissociation of dicumyl peroxide at M06-2X/aug-cc-pVDZ level.

Species	Lowest Energy excitation		Highest intensity excitation	
	λ (nm)	Oscillator strength	λ (nm)	Oscillator strength
M1	369.46	0.0008	181.91	0.0377
M2	236.53	0.0366	183.85	0.4821
M3	290.69	0.0005	200.88	0.0327
M4	397.75	0.0053	271.91	0.2569
M5	418.93	0.0014	180.56	0.1557
M6	350.67	0.0011	237.01	0.2604
M7	262.86	0.0095	176.30	0.5929
M8	418.93	0.0014	197.28	0.1583
M9	467.01	0.0006	352.97	0.0636
M10	450.64	0.0393	176.30	0.5929
M11	247.60	0.2808	181.51	0.3023
M12	229.45	0.0007	182.70	0.5567
M13	498.52	0.0016	307.29	0.0299
M14	624.02	0.0011	180.23	0.6109
M15	425.59	0.0012	197.46	0.0588
M16	562.91	0.0028	223.23	0.0665
M17	332.02	0.0398	332.02	0.0398
M18	501.41	0.0063	360.98	0.1447
M19	575.57	0.0008	323.02	0.1327
M20	527.29	0.0006	382.86	0.1755
M21	422.57	0.0081	257.59	0.1481
M22	413.19	0.0004	231.69	0.0417
M23	505.53	0.0024	306.12	0.0307
M24	486.91	0.0028	180.23	0.6109
M25	342.56	0.0589	342.56	0.0589
M26	431.48	0.0002	259.41	0.0310

The shifts in the energy of the important low energy excitation peaks of initial radical and first reaction products upon solvation in acetonitrile and ethanol are listed in table 2.18.

Table 2.18: Shift in the excitation energy of dicumyl peroxide dissociation radicals upon solvation in acetonitrile and ethanol.

Species	Excitation peak position (nm)	Excitation peak shift (nm)	
		In acetonitrile	In ethanol
M1	184	-1	0
M2	225	+5	+5
M3	229	-9	-8
M4	268	+8	+8
M5	182	-2	-2
M15	189	-6	-6

As it can be seen in table 2.18, also in case of radicals involved in the dissociation of dicumyl peroxide, TDDFT/PCM calculations are not showing large changes in the position of absorption peaks.

Chapter 3

CONCLUSIONS

Energy landscapes in photodissociation of diethyl peroxide, di-tert-butyl peroxide, and dicumyl peroxide were studied. Our results show that main reaction of peroxides decomposition can be identified by using DFT method for locating the transition states on the potential energy surface.

Among the compared functionals (SVWN, BLYP, TPSS, B3LYP and M06-2X), which have various degrees of approximation, M06-2X was found to be most suitable by considering its accuracy in calculations of equilibrium geometries, relative energies, and electronic excitation energies.

DFT method using M06-2X functional with aug-cc-pVDZ basis set in comparison with 6-31g(d,p), 6-311g(d,p), 6-311g(2d,2p), cc-pVDZ, cc-pVTZ, aug-cc-pVDZ, aug-cc-pVTZ, def2-SVP, and def2-TZVP basis sets was found to be adequately efficient by comparing equilibrium geometries, O-O bond dissociation energies, electronic excitation energies, and computation runtime.

DFT method using M06-2X functional with aug-cc-pVDZ basis shows sufficient accuracy for relative energy calculations in the studied systems in comparison with higher accuracy CCSD(T) method.

In our computations, the current parallel implementation of TDDFT code in Gaussian 09 package determined to be efficient and Hyper-Threading was found to decrease the computational performance due to various bottle-necks in shared system resources.

As it has already observed experimentally, methyl radical abstraction is the main dissociation mechanism for studied peroxides (diethyl peroxide, di-tert-butyl peroxide,

and dicumyl peroxide) after O-O bond breaking. This reaction was found to have the least activation energy in all studied systems.

Shifts in electronic excitation energies of studied radicals in acetonitrile and ethanol were found to be similar and negligible in PCM/TDDFT calculations. These solvents were found to be more effective on intensities of electronic excitation peaks. Therefore, if ethanol and acetonitrile solvents do not incorporate in the dissociation reactions of peroxides, their effects on UV-Vis absorption spectra can be neglected for characterization purpose and gas phase calculations can be safely used to interpret and compare the result obtained from solvent phase experiments.

Increase in the size of peroxide molecule and involved atoms number results in increase of PES complexity and introduces many new reaction pathways which make it harder to completely study all the possible reactions.

In study of radicals involved in dissociation of dicumyl peroxide we observed that most of the radicals with radical center on aromatic ring have electronic excitation in visible wavelengths.

BIBLIOGRAPHY

[1] Moss, G.P., Smith, P.A.S., and Tavernier, D. 1995. “Glossary of class names of organic compounds and reactivity intermediates based on structure (IUPAC Recommendations 1995)”, Pure and Applied Chemistry, 67, 1307-1375.

[2] Margolis, L.Y. 1963. Catalytic Oxidation of Hydrocarbons. In Advances in Catalysis, H.P. D.D. Eley and B.W. Paul, eds. (Academic Press), pp 429-501.

[3] Baxendale, J.H., Evans, M.G., and Park, C.S. 1946. “The mechanism and kinetics of the initiation of polymerisation by systems containing hydrogen peroxide”, Transactions of the Faraday Society, 42, 155-169.

[4] Dluzneski, P.R. 2001. “Peroxide Vulcanization of Elastomers”, Rubber Chemistry and Technology, 74, 451-492.

[5] Gray, J.I. 1978. “Measurement of lipid oxidation: A review”, Journal of the American Oil Chemists’ Society, 55, 539-546.

[6] Dickey, F.H., Cleland, G.H., and Lotz, C. 1949. “The Rôle of Organic Peroxides in the Induction of Mutations”, Proceedings of the National Academy of Sciences of the United States of America, 35, 581-586.

[7] Imlay, J.A., Chin, S.M., and Linn, S. 1988. “Toxic DNA damage by hydrogen peroxide through the Fenton reaction in vivo and in vitro”, Science, 240, 640-642.

[8] Bair, R.A., and Goddard, W.A. 1982. “Ab initio studies of the structures of peroxides and peroxy radicals”, Journal of the American Chemical Society, 104, 2719-2724.

[9] Jonsson, M. 1996. “Thermochemical Properties of Peroxides and Peroxyl Radicals”, The Journal of Physical Chemistry, 100, 6814-6818.

[10] Benassi, R., and Taddei, F. 1994. “Homolytic bond-dissociation in peroxides, peroxyacids, peroxyesters and related radicals: ab-initio MO calculations”, Tetrahedron, 50, 4795-4810.

[11] Bach, R.D., Ayala, P.Y., and Schlegel, H.B. 1996. “A Reassessment of the Bond Dissociation Energies of Peroxides. An ab Initio Study”, Journal of the American Chemical Society, 118, 12758-12765.

[12] Brown, D.J. 1948. “The Thermal Decomposition of Benzoyl Peroxide”, Journal of the American Chemical Society, 70, 1208-1209.

[13] Rembaum, A., and Szwarc, M. 1954. “Kinetics of the Thermal Decomposition of Diacetyl Peroxide. I. Gaseous Phase”, Journal of the American Chemical Society, 76, 5975-5978.

[14] Bailey, H.C., and Godin, G.W. 1956. “The thermal decomposition of dibenzoyl and di-α-cumyl peroxides in cumene”, Transactions of the Faraday Society, 52, 68-73.

[15] Hanst, P.L., and Calvert, J.G. 1959. “The Thermal Decomposition of Dimethyl Peroxide: The Oxygen–Oxygen Bond Strength of Dialkyl Peroxides”, The Journal of Physical Chemistry, 63, 104-107.

[16] Hoare, D.E., Protheroe, J.B., and Walsh, A.D. 1959. “The thermal decomposition of hydrogen peroxide vapour”, Transactions of the Faraday Society, 55, 548-557.

[17] Zewail, A.H. 2000. “Femtochemistry: Atomic-Scale Dynamics of the Chemical Bond”, The Journal of Physical Chemistry A, 104, 5660-5694.

[18] Aßmann, J., Kling, M., and Abel, B. 2003. “Watching Photoinduced Chemistry and Molecular Energy Flow in Solution in Real Time”, Angewandte Chemie International Edition, 42, 2226-2246.

[19] Buback, M., Kling, M., Schmatz, S., and Schroeder, J. 2004. “Photo-induced decomposition of organic peroxides: Ultrafast formation and decarboxylation of carbonyloxy radicals”, Physical Chemistry Chemical Physics, 6, 5441-5455.

[20] Buback, M., Kling, M., Seidel, M.T., Schott, F.D., Schroeder, J., and Steegmüller, U. 2001. “Picosecond IR Study of UV-Induced Peroxide Decomposition: Formation and Vibrational Relaxation of CO_2 in CH_2Cl_2 Solution”, Zeitschrift für Physikalische Chemie, 215, 717-735.

[21] Abel, B., Buback, M., Kling, M., Schmatz, S., and Schroeder, J. 2003. "A Seemingly Well Understood Light-Induced Peroxide Decarboxylation Reaction Reinvestigated with Femtosecond Time Resolution", Journal of the American Chemical Society, 125, 13274-13278.

[22] Abel, B., Assmann, J., Botschwina, P., Buback, M., Kling, M., Oswald, R., Schmatz, S., Schroeder, J., and Witte, T. 2003. "Experimental and Theoretical Investigations of the Ultrafast Photoinduced Decomposition of Organic Peroxides in Solution: Formation and Decarboxylation of Benzoyloxy Radicals", The Journal of Physical Chemistry A, 107, 5157-5167.

[23] Kling, M., and Schmatz, S. 2003. "Decarboxylation of carbonyloxy radicals: a density functional study", Physical Chemistry Chemical Physics, 5, 3891-3896.

[24] Abel, B., Aßmann, J., Buback, M., Kling, M., Schmatz, S., and Schroeder, J. 2003. "Ultrafast Decarboxylation of Organic Peroxides in Solution: Interplay of Different Spectroscopic Techniques, Quantum Chemistry, and Theoretical Modeling", Angewandte Chemie International Edition, 42, 299-303.

[25] Schrödinger, E. 1926. "Quantisierung als Eigenwertproblem", Annalen der Physik, 384, 361-376.

[26] Born, M., and Oppenheimer, R. 1927. "Zur Quantentheorie der Molekeln", Annalen der Physik, 389, 457-484.

[27] Hartree, D.R. 1928. "The Wave Mechanics of an Atom with a Non-Coulomb Central Field. Part I. Theory and Methods", Mathematical Proceedings of the Cambridge Philosophical Society, 24, 89-110.

[28] Fock, V. 1930. "Näherungsmethode zur Lösung des quantenmechanischen Mehrkörperproblems", Zeitschrift für Physik, 61, 126-148.

[29] Slater, J.C. 1929. "The Theory of Complex Spectra", Physical Review, 34, 1293-1322.

[30] Pauli, W. 1925. "Über den Zusammenhang des Abschlusses der Elektronengruppen im Atom mit der Komplexstruktur der Spektren", Zeitschrift für Physik, 31, 765-783.

[31] Harris, J. 1985. “Simplified method for calculating the energy of weakly interacting fragments”, Physical Review B, 31, 1770-1779.

[32] Hoffmann, R. 1963. “An Extended Hückel Theory. I. Hydrocarbons”, The Journal of Chemical Physics, 39, 1397-1412.

[33] Roothaan, C.C.J. 1951. “New Developments in Molecular Orbital Theory”, Reviews of Modern Physics, 23, 69-89.

[34] Hall, G.G. 1951. “The Molecular Orbital Theory of Chemical Valency. VIII. A Method of Calculating Ionization Potentials”, Proceedings of the Royal Society of London Series A: Mathematical and physical sciences, 205, 541-552.

[35] Eckart, C. 1930. “The Theory and Calculation of Screening Constants”, Physical Review, 36, 878-892.

[36] Møller, C., and Plesset, M.S. 1934. “Note on an Approximation Treatment for Many-Electron Systems”, Physical Review, 46, 618-622.

[37] Hylleraas, E.A. 1928. “Über den Grundzustand des Heliumatoms”, Zeitschrift für Physik, 48, 469-494.

[38] Čížek, J. 1966. “On the Correlation Problem in Atomic and Molecular Systems. Calculation of Wavefunction Components in Ursell-Type Expansion Using Quantum-Field Theoretical Methods”, The Journal of Chemical Physics, 45, 4256-4266.

[39] Paldus, J., Čížek, J., and Shavitt, I. 1972. “Correlation Problems in Atomic and Molecular Systems. IV. Extended Coupled-Pair Many-Electron Theory and Its Application to the BH_3 Molecule”, Physical Review A, 5, 50-67.

[40] Hohenberg, P., and Kohn, W. 1964. “Inhomogeneous Electron Gas”, Physical Review, 136, B864-B871.

[41] Kohn, W., and Sham, L.J. 1965. “Self-Consistent Equations Including Exchange and Correlation Effects”, Physical Review, 140, A1133-A1138.

[42] Lieb, E.H. 1983. “Density functionals for coulomb systems”, International Journal of Quantum Chemistry, 24, 243-277.

[43] Kurth, S., and Perdew, J.P. 2000. “Role of the exchange–correlation energy: Nature's glue”, International Journal of Quantum Chemistry, 77, 814-818.

[44] Oliphant, N., and Bartlett, R.J. 1994. “A systematic comparison of molecular properties obtained using Hartree–Fock, a hybrid Hartree–Fock density-functional-theory, and coupled-cluster methods”, The Journal of Chemical Physics, 100, 6550-6561.

[45] Le Bris, C. 2005. “Computational chemistry from the perspective of numerical analysis”, Acta Numerica, 14, 363-444.

[46] Challacombe, M., and Schwegler, E. 1997. “Linear scaling computation of the Fock matrix”, The Journal of Chemical Physics, 106, 5526-5536.

[47] Valiev, M., Bylaska, E.J., Govind, N., Kowalski, K., Straatsma, T.P., Van Dam, H.J.J., Wang, D., Nieplocha, J., Apra, E., Windus, T.L., et al. 2010. “NWChem: A comprehensive and scalable open-source solution for large scale molecular simulations”, Computer Physics Communications, 181, 1477-1489.

[48] Langreth, D.C., and Mehl, M.J. 1983. “Beyond the local-density approximation in calculations of ground-state electronic properties”, Physical Review B, 28, 1809-1834.

[49] Peverati, R., and Truhlar, D.G. 2012. “Exchange–Correlation Functional with Good Accuracy for Both Structural and Energetic Properties while Depending Only on the Density and Its Gradient”, Journal of Chemical Theory and Computation, 8, 2310-2319.

[50] Tao, J., Perdew, J.P., Staroverov, V.N., and Scuseria, G.E. 2003. “Climbing the Density Functional Ladder: Nonempirical Meta–Generalized Gradient Approximation Designed for Molecules and Solids”, Physical Review Letters, 91, 146401.

[51] Becke, A.D. 1993. “Density-functional thermochemistry. III. The role of exact exchange”, The Journal of Chemical Physics, 98, 5648-5652.

[52] Iikura, H., Tsuneda, T., Yanai, T., and Hirao, K. 2001. “A long-range correction scheme for generalized-gradient-approximation exchange functionals”, The Journal of Chemical Physics, 115, 3540-3544.

[53] Becke, A.D. 1996. “Density-functional thermochemistry. IV. A new dynamical correlation functional and implications for exact-exchange mixing”, The Journal of Chemical Physics, 104, 1040-1046.

[54] Bloch, F. 1929. “Über die Quantenmechanik der Elektronen in Kristallgittern”, Zeitschrift für Physik, 52, 555-600.

[55] Slater, J.C. 1930. “Atomic Shielding Constants”, Physical Review, 36, 57-64.

[56] Boys, S.F. 1950. “Electronic Wave Functions. I. A General Method of Calculation for the Stationary States of Any Molecular System”, Proceedings of the Royal Society of London Series A: Mathematical and physical sciences, 200, 542-554.

[57] Kato, T. 1957. “On the eigenfunctions of many-particle systems in quantum mechanics”, Communications on Pure and Applied Mathematics, 10, 151-177.

[58] Hehre, W.J., Stewart, R.F., and Pople, J.A. 1969. “Self-Consistent Molecular-Orbital Methods. I. Use of Gaussian Expansions of Slater-Type Atomic Orbitals”, The Journal of Chemical Physics, 51, 2657-2664.

[59] Krishnan, R., Binkley, J.S., Seeger, R., and Pople, J.A. 1980. “Self-consistent molecular orbital methods. XX. A basis set for correlated wave functions”, The Journal of Chemical Physics, 72, 650-654.

[60] Dunning, T.H. 1989. “Gaussian basis sets for use in correlated molecular calculations. I. The atoms boron through neon and hydrogen”, The Journal of Chemical Physics, 90, 1007-1023.

[61] Kendall, R.A., Dunning, T.H., and Harrison, R.J. 1992. “Electron affinities of the first-row atoms revisited. Systematic basis sets and wave functions”, The Journal of Chemical Physics, 96, 6796-6806.

[62] Weigend, F., and Ahlrichs, R. 2005. “Balanced basis sets of split valence, triple zeta valence and quadruple zeta valence quality for H to Rn: Design and assessment of accuracy”, Physical Chemistry Chemical Physics, 7, 3297-3305.

[63] Sun, J.Q., and Ruedenberg, K. 1993. “Quadratic steepest descent on potential energy surfaces. I. Basic formalism and quantitative assessment”, The Journal of Chemical Physics, 99, 5257-5268.

[64] Fletcher, R., and Reeves, C.M. 1964. “Function minimization by conjugate gradients”, The Computer Journal, 7, 149-154.

[65] Filippone, F., Meloni, S., and Parrinello, M. 2001. “A novel implicit Newton–Raphson geometry optimization method for density functional theory calculations”, The Journal of Chemical Physics, 115, 636-642.

[66] Fogarasi, G., Zhou, X., Taylor, P.W., and Pulay, P. 1992. “The calculation of ab initio molecular geometries: efficient optimization by natural internal coordinates and empirical correction by offset forces”, Journal of the American Chemical Society, 114, 8191-8201.

[67] Pulay, P., and Fogarasi, G. 1992. “Geometry optimization in redundant internal coordinates”, The Journal of Chemical Physics, 96, 2856-2860.

[68] Baker, J., Kessi, A., and Delley, B. 1996. “The generation and use of delocalized internal coordinates in geometry optimization”, The Journal of Chemical Physics, 105, 192-212.

[69] Paizs, B., Baker, J., Suhai, S., and Pulay, P. 2000. “Geometry optimization of large biomolecules in redundant internal coordinates”, The Journal of Chemical Physics, 113, 6566-6572.

[70] Eckert, F., Pulay, P., and Werner, H.-J. 1997. “Ab initio geometry optimization for large molecules”, Journal of Computational Chemistry, 18, 1473-1483.

[71] McIver, J.W., and Komornicki, A. 1972. “Structure of transition states in organic reactions. General theory and an application to the cyclobutene-butadiene isomerization using a semiempirical molecular orbital method”, Journal of the American Chemical Society, 94, 2625-2633.

[72] Schlegel, H.B. 2011. “Geometry optimization”, Wiley Interdisciplinary Reviews: Computational Molecular Science, 1, 790-809.

[73] Henkelman, G., and Jónsson, H. 2000. “Improved tangent estimate in the nudged elastic band method for finding minimum energy paths and saddle points”, The Journal of Chemical Physics, 113, 9978-9985.

[74] Halgren, T.A., and Lipscomb, W.N. 1977. “The synchronous-transit method for determining reaction pathways and locating molecular transition states”, Chemical Physics Letters, 49, 225-232.

[75] Schlegel, H.B. 1982. “Optimization of equilibrium geometries and transition structures”, Journal of Computational Chemistry, 3, 214-218.

[76] Quapp, W., and Heidrich, D. 1984. “Analysis of the concept of minimum energy path on the potential energy surface of chemically reacting systems”, Theoretica chimica acta, 66, 245-260.

[77] Fukui, K. 1970. “Formulation of the reaction coordinate”, The Journal of Physical Chemistry, 74, 4161-4163.

[78] Taketsugu, T., and Gordon, M.S. 1995. “Dynamic reaction path analysis based on an intrinsic reaction coordinate”, The Journal of Chemical Physics, 103, 10042-10049.

[79] Bishop, D.M., and Randič, M. 1966. “Ab Initio Calculation of Harmonic Force Constants”, The Journal of Chemical Physics, 44, 2480-2487.

[80] Pulay, P. 1969. “Ab initio calculation of force constants and equilibrium geometries in polyatomic molecules”, Molecular Physics, 17, 197-204.

[81] Feynman, R.P. 1939. “Forces in Molecules”, Physical Review, 56, 340-343.

[82] Hellmann, H. 2015. ”Hans Hellmann: Einführung in die Quantenchemie”.(Berlin Heidelberg: Springer).

[83] Hafner, J. 2003. “Vibrational spectroscopy using ab initio density-functional techniques”, Journal of Molecular Structure, 651–653, 3-17.

[84] Grev, R.S., Janssen, C.L., and Schaefer, H.F. 1991. “Concerning zero-point vibrational energy corrections to electronic energies”, The Journal of Chemical Physics, 95, 5128-5132.

[85] Scott, A.P., and Radom, L. 1996. “Harmonic Vibrational Frequencies: An Evaluation of Hartree−Fock, Møller−Plesset, Quadratic Configuration Interaction, Density Functional Theory, and Semiempirical Scale Factors”, The Journal of Physical Chemistry, 100, 16502-16513.

[86] Pople, J.A., Schlegel, H.B., Krishnan, R., Defrees, D.J., Binkley, J.S., Frisch, M.J., Whiteside, R.A., Hout, R.F., and Hehre, W.J. 1981. “Molecular orbital studies of vibrational frequencies”, International Journal of Quantum Chemistry, 20, 269-278.

[87] Hirata, S., Head-Gordon, M., and Bartlett, R.J. 1999. “Configuration interaction singles, time-dependent Hartree–Fock, and time-dependent density functional theory for the electronic excited states of extended systems”, The Journal of Chemical Physics, 111, 10774-10786.

[88] Brillouin, L.o. 1933. ”La méthode du champ self-consistent”.(Paris Hermann).

[89] Foresman, J.B., Head-Gordon, M., Pople, J.A., and Frisch, M.J. 1992. “Toward a systematic molecular orbital theory for excited states”, The Journal of Physical Chemistry, 96, 135-149.

[90] Dirac, P.A.M. 1930. “Note on Exchange Phenomena in the Thomas Atom”, Mathematical Proceedings of the Cambridge Philosophical Society, 26, 376-385.

[91] Runge, E., and Gross, E.K.U. 1984. “Density-Functional Theory for Time-Dependent Systems”, Physical Review Letters, 52, 997-1000.

[92] Gross, E.K.U., and Kohn, W. 1985. “Local density-functional theory of frequency-dependent linear response”, Physical Review Letters, 55, 2850-2852.

[93] Roos, B. 1972. “A new method for large-scale Cl calculations”, Chemical Physics Letters, 15, 153-159.

[94] Gilbert, T.L. 1972. “Multiconfiguration Self-Consistent-Field Theory for Localized Orbitals. I. The Orbital Equations”, Physical Review A, 6, 580-600.

[95] Roos, B.O., and Taylor, P.R. 1980. “A complete active space SCF method (CASSCF) using a density matrix formulated super-CI approach”, Chemical Physics, 48, 157-173.

[96] Andersson, K., Malmqvist, P.A., Roos, B.O., Sadlej, A.J., and Wolinski, K. 1990. “Second-order perturbation theory with a CASSCF reference function”, The Journal of Physical Chemistry, 94, 5483-5488.

[97] Crawford, T.D., Stanton, J.F., Allen, W.D., and Schaefer, H.F. 1997. “Hartree–Fock orbital instability envelopes in highly correlated single-reference wave functions”, The Journal of Chemical Physics, 107, 10626-10632.

[98] Hirata, S., and Head-Gordon, M. 1999. “Time-dependent density functional theory for radicals: An improved description of excited states with substantial double excitation character”, Chemical Physics Letters, 302, 375-382.

[99] Stratmann, R.E., Scuseria, G.E., and Frisch, M.J. 1998. “An efficient implementation of time-dependent density-functional theory for the calculation of excitation energies of large molecules”, The Journal of Chemical Physics, 109, 8218-8224.

[100] Furche, F., and Ahlrichs, R. 2002. “Adiabatic time-dependent density functional methods for excited state properties”, The Journal of Chemical Physics, 117, 7433-7447.

[101] Burdick, W.R., Saad, Y., Kronik, L., Vasiliev, I., Jain, M., and Chelikowsky, J.R. 2003. “Parallel implementation of time-dependent density functional theory”, Computer Physics Communications, 156, 22-42.

[102] Cossi, M., and Barone, V. 2001. “Time-dependent density functional theory for molecules in liquid solutions”, The Journal of Chemical Physics, 115, 4708-4717.

[103] Tomasi, J., and Persico, M. 1994. “Molecular Interactions in Solution: An Overview of Methods Based on Continuous Distributions of the Solvent”, Chemical Reviews, 94, 2027-2094.

[104] Mennucci, B., and Tomasi, J. 1997. “Continuum solvation models: A new approach to the problem of solute’s charge distribution and cavity boundaries”, The Journal of Chemical Physics, 106, 5151-5158.

[105] Miertuš, S., Scrocco, E., and Tomasi, J. 1981. “Electrostatic interaction of a solute with a continuum. A direct utilizaion of ab initio molecular potentials for the prevision of solvent effects”, Chemical Physics, 55, 117-129.

[106] Tomasi, J., Cammi, R., Mennucci, B., Cappelli, C., and Corni, S. 2002. "Molecular properties in solution described with a continuum solvation model", Physical Chemistry Chemical Physics, 4, 5697-5712.

[107] Cossi, M., Scalmani, G., Rega, N., and Barone, V. 2002. "New developments in the polarizable continuum model for quantum mechanical and classical calculations on molecules in solution", The Journal of Chemical Physics, 117, 43-54.

[108] Pomelli, C.S., Tomasi, J., and Barone, V. 2001. "An improved iterative solution to solve the electrostatic problem in the polarizable continuum model", Theoretical Chemistry Accounts, 105, 446-451.

[109] Scalmani, G., Barone, V., Kudin, K.N., Pomelli, C.S., Scuseria, G.E., and Frisch, M.J. 2004. "Achieving linear-scaling computational cost for the polarizable continuum model of solvation", Theoretical Chemistry Accounts, 111, 90-100.

[110] Fortunelli, A., and Tomasi, J. 1994. "The implementation of density functional theory within the polarizable continuum model for solvation", Chemical Physics Letters, 231, 34-39.

[111] Cossi, M., Barone, V., Cammi, R., and Tomasi, J. 1996. "Ab initio study of solvated molecules: a new implementation of the polarizable continuum model", Chemical Physics Letters, 255, 327-335.

[112] Karlström, G., Lindh, R., Malmqvist, P.-Å., Roos, B.O., Ryde, U., Veryazov, V., Widmark, P.-O., Cossi, M., Schimmelpfennig, B., Neogrady, P., et al. 2003. "MOLCAS: a program package for computational chemistry", Computational Materials Science, 28, 222-239.

[113] Aidas, K., Angeli, C., Bak, K.L., Bakken, V., Bast, R., Boman, L., Christiansen, O., Cimiraglia, R., Coriani, S., Dahle, P., et al. 2014. "The Dalton quantum chemistry program system", Wiley Interdisciplinary Reviews: Computational Molecular Science, 4, 269-284.

[114] Whitfield, J.D., Love, P.J., and Aspuru-Guzik, A. 2013. "Computational complexity in electronic structure", Physical Chemistry Chemical Physics, 15, 397-411.

[115] Schuch, N., and Verstraete, F. 2009. “Computational complexity of interacting electrons and fundamental limitations of density functional theory”, Nature Physics, 5, 732-735.

[116] Becke, A.D. 1993. “A new mixing of Hartree–Fock and local density-functional theories”, The Journal of Chemical Physics, 98, 1372-1377.

[117] Kendall, R.A., Aprà, E., Bernholdt, D.E., Bylaska, E.J., Dupuis, M., Fann, G.I., Harrison, R.J., Ju, J., Nichols, J.A., Nieplocha, J., et al. 2000. “High performance computational chemistry: An overview of NWChem a distributed parallel application”, Computer Physics Communications, 128, 260-283.

[118] Brode, S., Horn, H., Ehrig, M., Moldrup, D., Rice, J.E., and Ahlrichs, R. 1993. “Parallel direct SCF and gradient program for workstation clusters”, Journal of Computational Chemistry, 14, 1142-1148.

[119] Antony, J., Rendell, A.P., Yang, R., Trucks, G., and Frisch, M.J. 2011. “Modelling the Runtime of the Gaussian Computational Chemistry Application and Assessing the Impacts of Microarchitectural Variations”, Procedia Computer Science, 4, 281-291.

[120] Sousa, S.F., Fernandes, P.A., and Ramos, M.J. 2007. “General Performance of Density Functionals”, The Journal of Physical Chemistry A, 111, 10439-10452.

[121] Lee, C., Yang, W., and Parr, R.G. 1988. “Development of the Colle-Salvetti correlation-energy formula into a functional of the electron density”, Physical Review B, 37, 785-789.

[122] Martin, J.M.L., El-Yazal, J., and François, J.-P. 1995. “Basis set convergence and performance of density functional theory including exact exchange contributions for geometries and harmonic frequencies”, Molecular Physics, 86, 1437-1450.

[123] Rassolov, V.A., Ratner, M.A., and Pople, J.A. 2000. “Electron correlation in chemical bonds”, The Journal of Chemical Physics, 112, 4014-4019.

[124] Schreiner, P.R. 2007. “Relative Energy Computations with Approximate Density Functional Theory—A Caveat!”, Angewandte Chemie International Edition, 46, 4217-4219.

[125] Kruse, H., Goerigk, L., and Grimme, S. 2012. “Why the Standard B3LYP/6-31G* Model Chemistry Should Not Be Used in DFT Calculations of Molecular Thermochemistry: Understanding and Correcting the Problem”, The Journal of Organic Chemistry, 77, 10824-10834.

[126] Zhao, Y., González-García, N., and Truhlar, D.G. 2005. “Benchmark Database of Barrier Heights for Heavy Atom Transfer, Nucleophilic Substitution, Association, and Unimolecular Reactions and Its Use to Test Theoretical Methods”, The Journal of Physical Chemistry A, 109, 2012-2018.

[127] Lynch, B.J., and Truhlar, D.G. 2001. “How Well Can Hybrid Density Functional Methods Predict Transition State Geometries and Barrier Heights?”, The Journal of Physical Chemistry A, 105, 2936-2941.

[128] Laurent, A.D., and Jacquemin, D. 2013. “TD-DFT benchmarks: A review”, International Journal of Quantum Chemistry, 113, 2019-2039.

[129] Zhao, Y., and Truhlar, D.G. 2008. “Density Functionals with Broad Applicability in Chemistry”, Accounts of Chemical Research, 41, 157-167.

[130] Zhao, Y., and Truhlar, D.G. 2006. “A new local density functional for main-group thermochemistry, transition metal bonding, thermochemical kinetics, and noncovalent interactions”, The Journal of Chemical Physics, 125, 194101.

[131] Peverati, R., and Truhlar, D.G. 2012. “M11-L: A Local Density Functional That Provides Improved Accuracy for Electronic Structure Calculations in Chemistry and Physics”, The Journal of Physical Chemistry Letters, 3, 117-124.

[132] Peverati, R., and Truhlar, D.G. 2012. “An improved and broadly accurate local approximation to the exchange-correlation density functional: The MN12-L functional for electronic structure calculations in chemistry and physics”, Physical Chemistry Chemical Physics, 14, 13171-13174.

[133] Zhao, Y., Schultz, N.E., and Truhlar, D.G. 2005. “Exchange-correlation functional with broad accuracy for metallic and nonmetallic compounds, kinetics, and noncovalent interactions”, The Journal of Chemical Physics, 123, 161103.

[134] Zhao, Y., Schultz, N.E., and Truhlar, D.G. 2006. “Design of Density Functionals by Combining the Method of Constraint Satisfaction with Parametrization for Thermochemistry, Thermochemical Kinetics, and Noncovalent Interactions”, Journal of Chemical Theory and Computation, 2, 364-382.

[135] Zhao, Y., and Truhlar, D.G. 2006. “Density Functional for Spectroscopy: No Long-Range Self-Interaction Error, Good Performance for Rydberg and Charge-Transfer States, and Better Performance on Average than B3LYP for Ground States”, The Journal of Physical Chemistry A, 110, 13126-13130.

[136] Zhao, Y., and Truhlar, D. 2008. “The M06 suite of density functionals for main group thermochemistry, thermochemical kinetics, noncovalent interactions, excited states, and transition elements: two new functionals and systematic testing of four M06-class functionals and 12 other functionals”, Theoretical Chemistry Accounts, 120, 215-241.

[137] Zhao, Y., and Truhlar, D.G. 2008. “Exploring the Limit of Accuracy of the Global Hybrid Meta Density Functional for Main-Group Thermochemistry, Kinetics, and Noncovalent Interactions”, Journal of Chemical Theory and Computation, 4, 1849-1868.

[138] Peverati, R., and Truhlar, D.G. 2011. “Improving the Accuracy of Hybrid Meta-GGA Density Functionals by Range Separation”, The Journal of Physical Chemistry Letters, 2, 2810-2817.

[139] Peverati, R., and Truhlar, D.G. 2012. “Screened-exchange density functionals with broad accuracy for chemistry and solid-state physics”, Physical Chemistry Chemical Physics, 14, 16187-16191.

[140] Leang, S.S., Zahariev, F., and Gordon, M.S. 2012. “Benchmarking the performance of time-dependent density functional methods”, The Journal of Chemical Physics, 136, -.

[141] Jacquemin, D., Perpète, E.A., Ciofini, I., and Adamo, C. 2010. “Assessment of Functionals for TD-DFT Calculations of Singlet−Triplet Transitions”, Journal of Chemical Theory and Computation, 6, 1532-1537.

[142] Jacquemin, D., Perpète, E.A., Ciofini, I., Adamo, C., Valero, R., Zhao, Y., and Truhlar, D.G. 2010. "On the Performances of the M06 Family of Density Functionals for Electronic Excitation Energies", Journal of Chemical Theory and Computation, 6, 2071-2085.

[143] Wheeler, S.E., and Houk, K.N. 2010. "Integration Grid Errors for Meta-GGA-Predicted Reaction Energies: Origin of Grid Errors for the M06 Suite of Functionals", Journal of Chemical Theory and Computation, 6, 395-404.

[144] Charaf-Eddin, A., Planchat, A., Mennucci, B., Adamo, C., and Jacquemin, D. 2013. "Choosing a Functional for Computing Absorption and Fluorescence Band Shapes with TD-DFT", Journal of Chemical Theory and Computation, 9, 2749-2760.

[145] Vosko, S.H., Wilk, L., and Nusair, M. 1980. "Accurate spin-dependent electron liquid correlation energies for local spin density calculations: a critical analysis", Canadian Journal of Physics, 58, 1200-1211.

[146] Becke, A.D. 1988. "Density-functional exchange-energy approximation with correct asymptotic behavior", Physical Review A, 38, 3098-3100.

[147] Perdew, J.P., and Schmidt, K. 2001. "Jacob's ladder of density functional approximations for the exchange-correlation energy", AIP Conference Proceedings, 577, 1-20.

[148] Perdew, J.P., Ruzsinszky, A., Tao, J., Staroverov, V.N., Scuseria, G.E., and Csonka, G.I. 2005. "Prescription for the design and selection of density functional approximations: More constraint satisfaction with fewer fits", The Journal of Chemical Physics, 123, 062201.

[149] Frisch, M.J., Trucks, G.W., Schlegel, H.B., Scuseria, G.E., Robb, M.A., Cheeseman, J.R., Scalmani, G., Barone, V., Mennucci, B., Petersson, G.A., et al. 2009. "Gaussian 09". In. (Wallingford, CT, USA, Gaussian, Inc.

[150] Hunt, R.H., Leacock, R.A., Peters, C.W., and Hecht, K.T. 1965. "Internal-Rotation in Hydrogen Peroxide: The Far-Infrared Spectrum and the Determination of the Hindering Potential", The Journal of Chemical Physics, 42, 1931-1946.

[151] Redington, R.L., Olson, W.B., and Cross, P.C. 1962. "Studies of Hydrogen Peroxide: The Infrared Spectrum and the Internal Rotation Problem", The Journal of Chemical Physics, 36, 1311-1326.

[152] Koput, J. 1986. "On the r_0^* structure and the torsional potential function of hydrogen peroxide", Journal of Molecular Spectroscopy, 115, 438-441.

[153] Flaud, J.M., Camy-Peyret, C., Johns, J.W.C., and Carli, B. 1989. "The far infrared spectrum of H_2O_2. First observation of the staggering of the levels and determination of the cis barrier", The Journal of Chemical Physics, 91, 1504-1510.

[154] Tonmunphean, S., Parasuk, V., and Karpfen, A. 2002. "The Torsional Potential of Dimethyl Peroxide: Still a Difficult Case for Theory", The Journal of Physical Chemistry A, 106, 438-446.

[155] Boys, S.F., and Bernardi, F. 1970. "The calculation of small molecular interactions by the differences of separate total energies. Some procedures with reduced errors", Molecular Physics, 19, 553-566.

[156] Luo, X., Fleming, P.R., and Rizzo, T.R. 1992. "Vibrational overtone spectroscopy of the $4\nu_{OH}+\nu_{OH'}$ combination level of HOOH via sequential local mode–local mode excitation", The Journal of Chemical Physics, 96, 5659-5667.

[157] Suto, M., and Lee, L.C. 1983. "OH($A^2\Sigma^+ \rightarrow X^2\prod$) yield from photodissociation of H_2O_2 at 106–193 nm", Chemical Physics Letters, 98, 152-156.

[158] Huber, K.P., and Herzberg , G. 1979. "Molecular Spectra and Molecular Structure".(Springer US).

[159] Jankowski, K., Becherer, R., Scharf, P., Schiffer, H., and Ahlrichs, R. 1985. "The impact of higher polarization basis functions on molecular ab initio results. I. The ground state of F2", The Journal of Chemical Physics, 82, 1413-1419.

[160] Wiberg, K.B., de Oliveira, A.E., and Trucks, G. 2002. "A Comparison of the Electronic Transition Energies for Ethene, Isobutene, Formaldehyde, and Acetone Calculated Using RPA, TDDFT, and EOM-CCSD. Effect of Basis Sets", The Journal of Physical Chemistry A, 106, 4192-4199.

[161] Bakken, V., and Helgaker, T. 2002. “The efficient optimization of molecular geometries using redundant internal coordinates”, The Journal of Chemical Physics, 117, 9160-9174.

[162] Baker, J. 1993. “Techniques for geometry optimization: A comparison of cartesian and natural internal coordinates”, Journal of Computational Chemistry, 14, 1085-1100.

[163] Ayala, P.Y., and Schlegel, H.B. 1997. “A combined method for determining reaction paths, minima, and transition state geometries”, The Journal of Chemical Physics, 107, 375-384.

[164] Peng, C., and Schlegel, H.B. 1993. “Combining Synchronous Transit and Quasi-Newton Methods to Find Transition States”, Israel Journal of Chemistry, 33, 449-454.

[165] Peng, C., Ayala, P.Y., Schlegel, H.B., and Frisch, M.J. 1996. “Using redundant internal coordinates to optimize equilibrium geometries and transition states”, Journal of Computational Chemistry, 17, 49-56.

[166] Gonzalez, C., and Schlegel, H.B. 1989. “An improved algorithm for reaction path following”, The Journal of Chemical Physics, 90, 2154-2161.

[167] Gonzalez, C., and Schlegel, H.B. 1990. “Reaction path following in mass-weighted internal coordinates”, The Journal of Physical Chemistry, 94, 5523-5527.

[168] Alecu, I.M., Zheng, J., Zhao, Y., and Truhlar, D.G. 2010. “Computational Thermochemistry: Scale Factor Databases and Scale Factors for Vibrational Frequencies Obtained from Electronic Model Chemistries”, Journal of Chemical Theory and Computation, 6, 2872-2887.

[169] Stephens, P.J., and Harada, N. 2010. “ECD cotton effect approximated by the Gaussian curve and other methods”, Chirality, 22, 229-233.

[170] Hu, Y., Li, W., and Hu, J. 2005. “Resolving overlapped spectra with curve fitting”, Spectrochimica Acta Part A: Molecular and Biomolecular Spectroscopy, 62, 16-21.

[171] Delley, B. 2010. “Time dependent density functional theory with DMol^3”, Journal of Physics: Condensed Matter, 22, 384208.

[172] Helmbold, D.P., and McDowell, C.E. 1990. “Modelling speedup (n) greater than n”, Parallel and Distributed Systems, IEEE Transactions on, 1, 250-256.

[173] Charles, J., Jassi, P., Ananth, N.S., Sadat, A., and Fedorova, A. 2009. “Evaluation of the Intel® Core™ i7 Turbo Boost feature”. In Workload Characterization, 2009 IISWC 2009 IEEE International Symposium on. 188-197.

[174] Gustafson, J.L. 1988. “Reevaluating Amdahl's Law”, Communications of the ACM, 31, 532-533.

[175] Magro, W., Petersen, P., and Shah, S. 2002. “Hyper-Threading Technology: Impact on Compute-Intensive Workloads”, Intel Technology Journal, 6, 1-9.

[176] Harris, E.J., and Egerton, A.C. 1938. “The Decomposition and Ignition of Peroxides. I. Diethylperoxide”, Proceedings of the Royal Society of London Series A, Mathematical and Physical Sciences, 168, 1-18.

[177] Zewail, A.H. 1988. “Laser Femtochemistry”, Science, 242, 1645-1653.

[178] Rebbert, R.E., and Laidler, K.J. 1952. “Kinetics of the Decomposition of Diethyl Peroxide”, The Journal of Chemical Physics, 20, 574-577.

[179] Armentrout, P.B., and Simons, J. 1992. “Understanding heterolytic bond cleavage”, Journal of the American Chemical Society, 114, 8627-8633.

[180] Luo, Y.-R., and Holmes, J.L. 1994. “Homo- and Heterolytic X-C Bond Energies. 2. Heterolytic Bond Energies in Unsaturated Organic Chain Compounds”, The Journal of Physical Chemistry, 98, 10368-10372.

[181] Pople, J.A., Head-Gordon, M., and Raghavachari, K. 1987. “Quadratic configuration interaction. A general technique for determining electron correlation energies”, The Journal of Chemical Physics, 87, 5968-5975.

[182] Wohlfarth, C. 2008. Dielectric constant of acetonitrile. In Supplement to IV/6, M.D. Lechner, ed. (Springer Berlin Heidelberg), pp 117-121.

[183] Wohlfarth, C. 2008. Dielectric constant of ethanol. In Supplement to IV/6, M.D. Lechner, ed. (Springer Berlin Heidelberg), pp 133-139.

[184] Dorer, F.H., and Johnson, S.N. 1971. "Energy Partitioning on Photolysis of Di-tert-butyl Peroxide", The Journal of Physical Chemistry, 75, 3651-3655.

[185] Atkinson, R. 1997. "Gas-Phase Tropospheric Chemistry of Volatile Organic Compounds: 1. Alkanes and Alkenes", Journal of Physical and Chemical Reference Data, 26, 215-290.

[186] Alvarez-Idaboy, J.R., Mora-Diez, N., and Vivier-Bunge, A. 2000. "A Quantum Chemical and Classical Transition State Theory Explanation of Negative Activation Energies in OH Addition To Substituted Ethenes", Journal of the American Chemical Society, 122, 3715-3720.

[187] Alvarez–Idaboy, J.R., Díaz–Acosta, I., and Vivier–Bunge, A. 1998. "Energetics of mechanism of OH-propene reaction at low pressures in inert atmosphere", Journal of Computational Chemistry, 19, 811-819.

[188] Norrish, R.G.W., and Searby, M.H. 1956. "The Photochemical Decomposition of Dicumyl Peroxide and Cumene Hydroperoxide in Solution", Proceedings of the Royal Society of London A: Mathematical, Physical and Engineering Sciences, 237, 464-475.

[189] Baignee, A., Howard, J.A., Scaiano, J.C., and Stewart, L.C. 1983. "Absolute rate constants for reactions of cumyloxy in solution", Journal of the American Chemical Society, 105, 6120-6123.

[190] Avila, D.V., Lusztyk, J., and Ingold, K.U. 1992. "Color benzyloxyl and cumyloxyl orange and 4-methoxycumyloxyl blue. Unexpected discovery that arylcarbinyloxyl radicals have strong absorptions in the visible", Journal of the American Chemical Society, 114, 6576-6577.

[191] Di Somma, I., Marotta, R., Andreozzi, R., and Caprio, V. 2012. "Dicumyl Peroxide Thermal Decomposition in Cumene: Development of a Kinetic Model", Industrial & Engineering Chemistry Research, 51, 7493-7499.

[192] Rajakumar, B., Flad, J.E., Gierczak, T., Ravishankara, A.R., and Burkholder, J.B. 2007. “Visible Absorption Spectrum of the CH_3CO Radical”, The Journal of Physical Chemistry A, 111, 8950-8958.